Universidade de Aveiro

2021

Filipe Silva de Matos

Biotintas inovadoras baseadas em alginato e micropartículas de acetato de celulose para aplicação em bio-impressão 3D

Novel alginate and cellulose acetate microparticles based bioinks for 3D bioprinting applications

Universidade de Aveiro

2021

Filipe Silva de Matos

Biotintas inovadoras baseadas em alginato e micropartículas de acetato de celulose para aplicação em bio-impressão 3D

Novel alginate and cellulose acetate microparticles based bioinks for 3D bioprinting applications

Dissertação apresentada à Universidade de Aveiro para cumprimento dos requisitos necessários à obtenção do grau de Mestre em Bioquímica, ramo Bioquímica Clínica, realizada sob a orientação científica da Doutora Carmen Sofia da Rocha Freire, Investigadora Principal com Agregação do Departamento de Química da Universidade de Aveiro e da Doutora Carla Andreia Cunha Vilela, Investigadora Auxiliar do Departamento de Química da Universidade de Aveiro.

Dedico esta dissertação à minha família e amigos. A eles devo tudo o que sou.

o júri

presidente

Professor Doutor Carlos Pedro Fontes Oliveira
Professor Auxiliar do Departamento de Química da Universidade de Aveiro

Doutor Gil Alberto Batista Gonçalves
Investigador Auxiliar do Departamento de Engenharia Mecânica da Universidade de Aveiro

Doutora Carmen Sofia da Rocha Freire
Investigadora Principal com Agregação do Departamento de Química da Universidade de Aveiro

agradecimentos

Esta dissertação não teria sido possível sem o apoio de várias pessoas, às quais passo a agradecer.

Em primeiro lugar quero agradecer às minhas orientadoras, Doutora Carmen Freire e Doutora Carla Vilela, pelo apoio que me prestaram. Obrigado por me ajudarem a tornar esta dissertação em algo real e por me apoiarem nesta área de que tanto aprendi a gostar.

Agradeço também a todos os colegas do laboratório BioPol4fun que de alguma forma contribuíram para a realização desta dissertação, com especial referência à Maria do Céu Teixeira, ao Doutor Nuno Silva, ao Doutor Ricardo Pinto, à Ana Silva e à Nicole Lameirinhas.

A todos os meus amigos que de certa forma fizeram de Aveiro a minha segunda casa, e sem os quais este percurso não teria o mesmo impacto que teve em mim, Daniela, Guilherme, Andreia, Bárbara e Telmo. Agradeço também aos meus amigos de Viana, Gonçalo, Diogo, Bruno, Hugo, Mariana, Matilde, Sara, Rui e Bruna que me acompanham desde sempre e sei que para sempre, e que de certa forma com o seu apoio contribuíram para esta dissertação.

Agradeço também à minha namorada Ana, que sempre me apoiou, nos bons e nos piores momentos, fazendo-me acreditar e dando-me força para atingir os meus objetivos.

Por fim, mas não menos importante, à minha família. À minha irmã Margarida, que independentemente da circunstância esteve sempre onde foi preciso para me apoiar, para me ajudar e para ouvir as minhas frustrações. Ao meu avô João, que de forma carinhosa e constante me apoiou em tudo o que fiz e em todas as minhas decisões. Aos meus pais, Eusébio e Teresa, que tornaram todo este percurso possível, com o seu amor, dedicação e esforço. A eles que me fizeram quem sou hoje, orgulhoso de mim próprio e do meu percurso. Sou eternamente grato por vos ter na minha vida.

palavras-chave

Bio-impressão 3D, biotintas, hidrogéis, micropartículas, alginato de sódio, acetato de celulose

resumo

O dano de tecidos e órgãos pode ocorrer por diversas razões, tais como lesão, doença ou falhas no seu desenvolvimento. A bio-impressão 3D surge como uma técnica inovadora para a produção de análogos de tecido vivos que podem ser usados na regeneração de tecidos danificados, no domínio da engenharia de tecidos. As biotintas são os materiais depositados pelas bio-impressoras e a sua escolha adequada é fundamental para o sucesso do processo de bio-impressão. Uma biotinta deve ter elevada capacidade de impressão, ser insolúvel no meio fisiológico, ter grande estabilidade mecânica, garantir uma taxa de degradação adequada, ser citocompatível e não imunogénica. Embora se tenham observado diversos avanços neste domínio, o desenvolvimento de biotintas com elevado desempenho mecânico e viabilidade celular é ainda uma das principais limitações nesta área. Desta forma, o objetivo desta dissertação é o desenvolvimento de uma nova biotinta do tipo microtransportadores à base de micropartículas de acetato de celulose e de um hidrogel de alginato de sódio, com propriedades mecânicas melhoradas e elevada viabilidade celular. O alginato foi escolhido devido à sua capacidade de formação de hidrogéis por reticulação com cloreto de cálcio e o acetato de celulose por ser um polímero abundante, com boas propriedades mecânicas e fácil de processar em micropartículas.

As micropartículas de acetato de celulose foram produzidas por regeneração, na qual o acetato de celulose é primeiramente dissolvido em acetona e posteriormente regenerado pela adição de água gota-a-gota. Estas partículas foram então caraterizadas quanto à sua composição química, morfologia, tamanho e citotoxicidade. As micropartículas mostraram ser não citotóxicas para os queratinócitos humanos (HaCaT), revelando todas taxas de viabilidade celular superiores a 75%. As tintas de alginato e micropartículas de acetato de celulose foram obtidas através da dispersão das micropartículas de acetato celulose (1%, 5% e 10% (m/m) relativamente à massa de alginato (m/m)) numa solução de alginato (4% (m/v)) e posterior pré-reticulação com uma solução de cloreto de cálcio a 0.5% (m/v). Todas as formulações foram caraterizadas em termos da sua reologia e aptidão à impressão. Todas as tintas revelaram um comportamento pseudoplástico, sendo este relevante para aplicações em bio-impressão 3D, apresentando também taxas de recuperação superiores a 85%. Nos ensaios de impressão 3D foram determinados os parâmetros ótimos de pressão (1,5 ou 2 bar), velocidade de impressão (8,5 ou 10 mm/s), diâmetro do bocal de impressão (0,25 mm) e do espaçamento entre filamentos (3 mm). Desta forma, foi possível imprimir até 6 camadas sem perda de resolução para a tinta com uma concentração de 10% de micropartículas. Estes resultados confirmam as potencialidades destas formulações para posterior incorporação de células para bio-impressão de análogos de tecidos de pele.

keywords

3D Bioprinting, bioinks, hydrogels, microparticles, sodium alginate, cellulose acetate

abstract

Tissue and organ damage can occur due to a variety of reasons, such as injury, disease, or failure to thrive. 3D-bioprinting emerged as an innovative technique to produce living tissue analogues that can be used in the regeneration of damaged tissues in the field of tissue engineering. Bioinks are the materials deposited by bioprinters, and their proper choice is fundamental for the success of the bioprinting process. A bioink must have high printability, be insoluble in the physiological medium, have great mechanical stability, guarantee a suitable degradation rate, and be cytocompatible and non-immunogenic. Although several advances in this field have been observed, the development of bioinks with high mechanical performance and cell viability is still one of the main limitations in this area. Thus, the objective of this dissertation is the development of a new microcarrier type bioink based on cellulose acetate microparticles and a sodium alginate hydrogel with improved mechanical properties and high cell viability. Alginate was chosen due to its ability to form hydrogels by cross-linking with calcium chloride and cellulose acetate because it is an abundant polymer with good mechanical properties, and it is easy to process into microparticles.

Cellulose acetate microparticles were produced via regeneration (water-on-polymer method), in which cellulose acetate is first dissolved in acetone and subsequently regenerated by drop-wise addition of water. These particles were then characterized in terms of chemical composition, morphology, size, and cytotoxicity. The microparticles showed to be non-cytotoxic to human keratinocyte (HaCaT) cells, revealing cell viability rates above 75%. The alginate and cellulose acetate microparticles inks were obtained by dispersing the cellulose acetate microparticles (1%, 5% and 10% with respect to the alginate mass (m/m)) in an alginate solution (4% (m/v)) followed by pre-crosslinking with a 0.5% (m/v) of calcium chloride solution. All formulations were characterized in terms of their rheology and printability. All inks showed a shear-thinning behaviour, which is relevant for applications in 3D-bioprinting, also presenting recovery rates above 85%. In the 3D-printing tests, the optimum parameters of pressure (1.5 or 2 bar), printing speed (8.5 or 10 mm/s), nozzle width (0.25 mm) and spacing between filaments (3 mm) were determined. In this way, it was possible to print up to 6 layers without loss of resolution for the ink with a concentration of 10% of microparticles. These results confirm the potential of these formulations for subsequent incorporation of cells for bioprinting of skin tissue analogues.

Abbreviations

CA	Cellulose acetate
CAD	Computer-aided design
CIJ	Continuous inkjet
CT	Computed tomography
DBB	Droplet-based bioprinting
dECM	Decellularized extracellular matrix
DLP	Digital light processing
DMEM	Dulbecco's Modified Eagle Medium
DOD	Drop-on-Demand inkjet
EBB	Extrusion-based bioprinting
ECM	Extracellular matrix
EDTA	Ethylenediaminetetraacetic acid
FBS	Fetal bovine serum
FTIR	Fourier-transform infrared spectroscopy
GelMA	Gelatin methacrylate
LBB	Laser-based bioprinting
LDW	Laser-based direct writing
LIFT	Laser-induced forward transfer
MRI	Magnetic resonance imaging
OPTN	Organ Procurement and Transplantation Network
PBB	Photocuring-based bioprinting
PCL	Polycaprolactone
PEG	Poly(ethylene glycol)
SDS	Sodium dodecyl sulfate

SLA	Stereolithography
STEM	Scanning transmission electron microscopy
UV	Ultra-violet

Table of Content

Contextualization

Bioprinting has been one of the most prominent subjects of research in the latter decade. Studies have been centered on the development of new bioinks and bioprinting methods to produce living tissues analogs (and organs) for several applications, including tissue engineering, drugs screening, and diseases research.[1] However, this technology still has much room for improvement since there are still some obstacles that have not yet been overcome.[2] For example, the development of bioinks with adequate mechanical properties and high cell viability at an accessible price is a critical limitation of the bioprinting approach.[3]

In this context, the objective of this work is to develop a novel biopolymeric microcarrier based bioink with improved mechanical properties and high cell viability taking advantage of the unique properties of cellulose acetate microparticles. The work comprised the production of the cellulose acetate microparticles and their characterization (morphology, structure, and in vitro cytotoxicity) and loading in an alginate hydrogel. The obtained inks were then submitted to rheologic characterization and 3D-bioprinting studies.

This dissertation is organized into three main parts. The first, second and third chapters are dedicated to introducing 3D-bioprinting regarding the different techniques and the various types of bioinks used for printing living tissue scaffolds. Then, the materials and methods section (chapter 4) is devoted to describing the materials and methodologies used during the experimental work. In chapter 5, the main results obtained in this study are presented and discussed, followed by the conclusions and future perspectives (chapter 6).

1. Introduction

Tissue and organ failures may occur due to disease, injury, and development effects. Organ and tissue transplants have proven to be one of the most effective ways to overcome this issue. However, the number of tissue and organ donors is much lower than the number of required transplants.[4] Based on Organ Procurement and Transplantation Network (OPTN) data as of November 16 (2020), in the United States of America, there were a total of 108.564 humans needing a transplant, for which there were only 15.157 donors.[5] Thus, it is necessary to look for new solutions for the problem associated with the scarcity of donors. Therefore, scientific research is increasingly focusing on human tissue engineering and regenerative medicine.[4,6]

Tissue engineering combines both the principles of engineering and life sciences, using living cells, biocompatible materials, and biochemical/physical factors toward the development of biological substitutes that can repair injuries or even replace a failing organ's function.[7,8] Tissue engineering emerged in mid-1933 when Bisceglie encased mouse tumour cells in a polymer membrane and inserted it into the abdominal cavity of a pig.[8] The mouse cells remained alive, proving that the pig's immune system did not kill them.[8] Tissue engineering research developed over the years. Later in the 1980s, approaches like replacing damaged skin with cells loaded in collagen gels or collagen-glycosaminoglycan composites to guide regeneration (Figure 1) were attempted.[8,9] At this time, tissue engineering was presented to the world, resulting in increasing interest by the scientific research community on this subject.[8] The need to create custom made scaffolds led to the development of technologies like 3D bioprinting.[10]

3D Bioprinting consists of fabricating 3D biological scaffolds by patterning and assembling living and non-living components, referred to as bioinks, in a predetermined and simulated 3D architecture.[10] Imaging techniques, such as magnetic resonance imaging (MRI), computed tomography (CT), and radiological diagnosis that provides a visual illustration of the precise 3D structures of organs and tissues, have been used as a reference for computer-aided design (CAD). CAD designs scaffolds capable of providing essential growing conditions to the cells and making it possible for the scaffold to differentiate into a tissue and then into a working organ.[10] These scaffolds are then created using a 3D bioprinter that deposits the bioink layer by layer, allowing the creation of complex structures with high precision in a short period of time.[10]

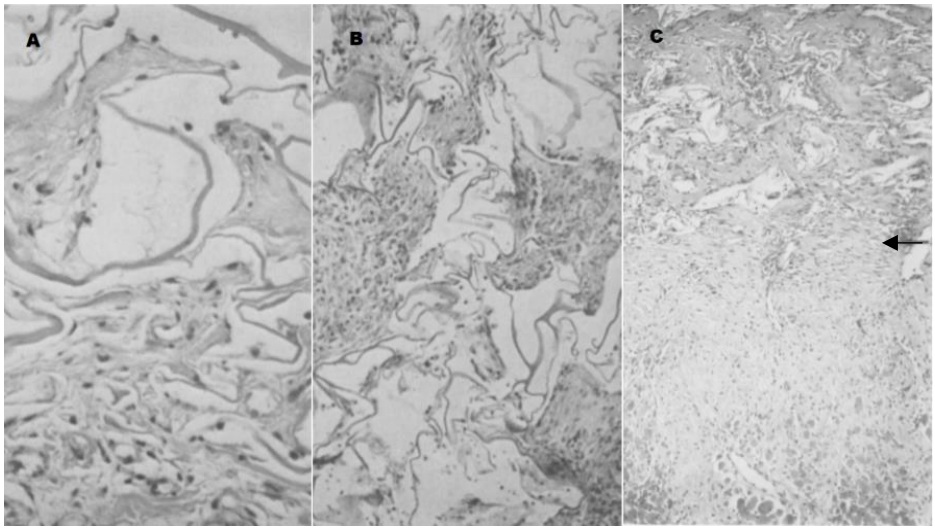

Figure 1 - Photomicrograph of grafted artificial skin; A) one week following artificial skin grafting with tufts of newly synthesized connective tissue matrix migrating into the artificial lattice; B) 14 days after grafting, there is extensive infiltration of cells, matrix, and vessels into the artificial dermal lattice; C) 5 weeks following implantation the junction between the artificial dermis and host bed is marked with an arrow. There is extensive infiltration of connective tissue matrix and vessels throughout the entire width of the artificial dermis. Adapted from Burke JF, *et al*. (1981).[9]

3D-bioprinting is also used to develop drug delivery systems by using hydrogels' ability to hold a significant amount of growth factors and drugs to release at the target site at a slow rate or to develop tissue models for new drugs screening.[1,11] This new technology has also proved helpful in tumour modelling by creating a 3D microenvironment for tumours to interact with stromal cells leading to a precise model which makes it possible to study tumour progression, drug response, intracellular and intercellular molecular interactions, and metastatic progression.[1]

The various 3D-bioprinting methods and the various types of bioinks are described in the following sections.

2. Bioprinting techniques

As mentioned above, 3D bioprinting can be described as the process of manipulating cell-laden bioinks to fabricate living structures able to be applied in regenerative medicine, cell biology, and pharmacokinetic studies. There are four main bioprinting methods, which differ in terms of prototyping principles, printing materials, cell viability, and cell density,

viz: extrusion-based (EBB), droplet-based (DBB), laser-based (LBB), and photocuring-based (PBB) bioprinting techniques.[12] In extrusion-based bioprinting, the bioink is extruded to form continuous filaments for building the constructs; on droplet-based bioprinting, droplets are produced and stacked into structures; laser-based bioprinting strategy stems from the laser-induced forward transfer (LIFT) effect, which allows to print different living cells and biomaterials with high precision and micrometer resolution; in photocuring-based bioprinting, photocurable materials are deposited, solidified and stacked layer-by-layer to achieve the final 3D models.[12,13]

2.1. Extrusion-based bioprinting (EBB)

Extrusion-based bioprinting is the most widely used bioprinting approach since it is versatile and affordable.[14] This method can be used to print biomaterials with different concentrations of cells and viscosities, thus becoming the preferred method by the scientific community for the construction of tissues with good mechanical properties.[12,15] Both dispensing and automated robotic systems can be used in which the bioink is extruded through a nozzle employing mechanical or pneumatic force, forming microfilaments that are deposited and stacked, forming the desired structures. Also, this method incorporates computer software, enabling the user to load a computer-aided design (CAD) file to print the structure automatically.[15]

The extrusion of the bioink can be achieved through different mechanisms, such as pneumatic, piston, and screw-driven mechanisms (Figure 2). Each mechanism has its advantages and disadvantages. The pneumatic-driven extrusion can be used for high-precision applications, finding its best use in polymeric based systems with high viscosity.[16] However, in this case, the deposition may be delayed thanks to the compressed gas. The piston-driven extrusion reveals itself to provide more control over the flow of the bioink through the nozzle, making it the best option regarding the control of deposition.[12,16]

Lastly, the screw-driven extrusion gives more volumetric control, being also beneficial for the extrusion of biomaterials with higher viscosities. Since this methodology involves much pressure, a careful design of the screw parts is required to avoid potential harm to the loaded cells.[15,17] Bioprinting approaches that combine both piston-driven and screw-driven have also been reported.[18] This combined method leads to better printability of semi-solid or

solid-state biomaterials. Devices that use these two methods tend to be more complex in terms of cleaning and disinfection, ending up being more expensive.[12,18]

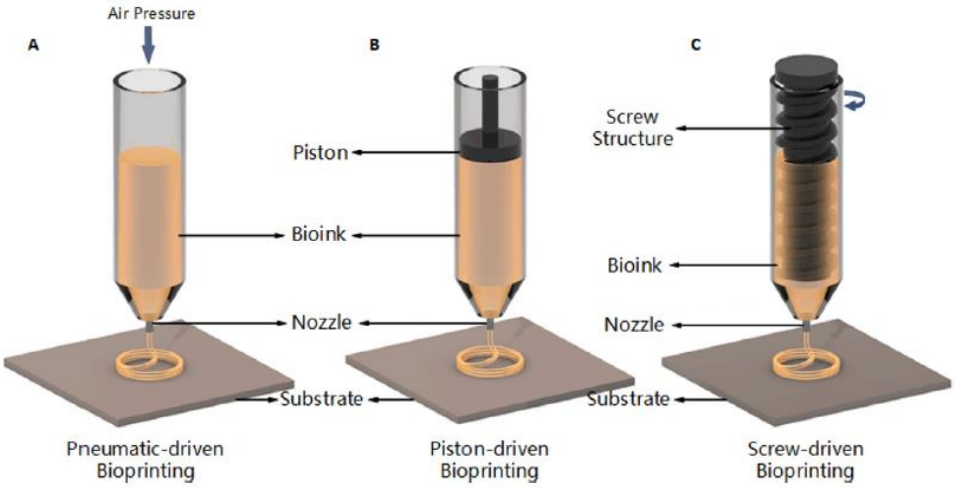

Figure 2 - Representation of different mechanism-driven extrusion bioprinting. (Adapted from Zeming Gu. *et al.*, 2019)[12].

2.2. Droplet-based bioprinting (DBB)

The droplet-based bioprinting is simple, agile, versatile, and allows deposition pattern control. This bioprinting method regards independent and discrete droplets as basic units, making it possible to precisely control biologics such as cells, growth factors, genes, etc., leading to high-resolution bioconstructs.[12,19] It also permits controlling specific properties, such as swelling and shrinkage of the construct, making the final product look closer to what is predictable.[19] This method can mediate the gelation process making it one of the best printing resolution methods.[19]

Apart from having various advantages compared to the other methods, droplet-based bioprinting has some limitations, with clogging being the most common.[19] Some bioinks accumulate at the nozzle leading to its obstruction. Therefore, in this case, it is essential to use bioinks with low viscosity, for example, low-viscosity hydrogels.[19] Due to the limited range of available bioinks materials with these requirements, DBB is not the best method to fabricate mechanically strong and structurally well-integrated constructs.[19,20]

This bioprinting method comprises three major categories, namely inkjet, acoustic and electrohydrodynamic bioprinting.[19] Inkjet bioprinting is said to be the first-ever bioprinting

method. This methodology involves two main steps: (1) the formation of discrete droplets which are deposited in specific substrate locations; and (2) the interaction that occurs between the droplets and the substrate. These droplets are dispensed with the help of gravity, atmospheric pressure, and the fluid mechanics of the bioink. Inkjet bioprinting can be further divided into two categories according to how the droplets are formed: continuous inkjet (CIJ) and Drop-on-Demand inkjet (DOD).[12,19,20] In CIJ, the bioink solution is forced through a nozzle, ending up broken into a stream of droplets. This phenomenon is characterized by transforming a stream of liquid into a discrete train of drops.[19] The stream of liquid is usually perturbed by various factors, including the potential energy owing to the surface energy of the jet and the kinetic energy associated with the jet's motion. That perturbation will eventually lead to the unrest of liquid streaming, breaking it up into a stream of droplets.[12] In contrast, DOD produces a droplet when required, making it easier to pattern biologics and control the process, also being more economically appealing.[20] This method makes it possible to achieve a smaller drop volume, leading to higher printing resolution. This method relies on three different mechanisms to generate droplets: piezoelectric inkjet, thermal inkjet, and electrostatic inkjet (Figure 3).[19] In piezoelectric inkjet, the piezoelectric actuator is struck by a voltage pulse, changing its form. This change in shape causes a modification in the volume of the fluid chamber resulting in a pressure wave leading to the release of a drop.[21] In thermal inkjet, the ink is heated up by a thermal actuator's action, resulting in the formation of an air bubble. This bubble rapidly explodes, resulting in a quick variation of the chamber's pressure leading to a drop ejection.[19,21] Finally, electrostatic inkjet bioprinting increases the volume of the fluid chamber thanks to a voltage pulse responsible for pressure plate bending, thus leading to the release of a single droplet.[22]

In contrast to inkjet bioprinting, in which the droplets are extruded from a nozzle, in acoustic-bioprinting, the droplet is ejected from an open pool, not exposing the bioink to harmful stressors such as voltage, pressure, or heat.[12,19] This technique relies on acoustic waves generated by the piezoelectric substrate and the gold rings, which are part of the acoustic actuator.[19,23] These waves will disturb the surface tension, resulting in the formation of a focal point close to the exit channel leading to the ejection of droplets.[19]

Lastly, in electrohydrodynamic bioprinting, instead of applying high pressure to dispense the bioink, which occasionally affects cell viability, as in the inkjet technique, this method uses an electric field. This electric field is originated from the high voltage applied

between the nozzle and the substrate.[12] Thanks to this electric field, electrostatic stresses overcome the surface tension of the bioink at the tip of the nozzle, resulting in the ejection of the droplet. This type of bioprinting allows the selection of a specific droplet stream mode and is also an ideal method for high viscosity/concentration bioinks and applications that may require small nozzles. Sometimes, the cell viability can end up being affected by the electric field but also by the bioink flow rate.[12,19]

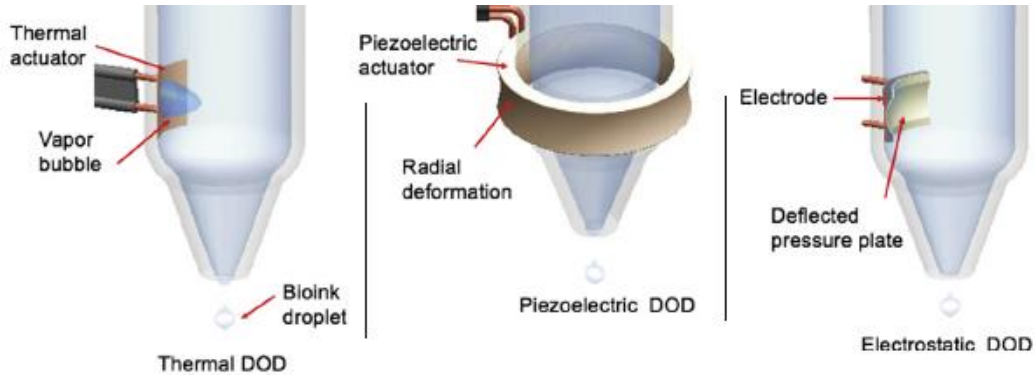

Figure 3– Representation of different Drop-on-Demand (DOD) bioprinting modalities. (Adapted from Hemanth Gudapati. *et al.*, 2016)[19].

2.3. Laser-based bioprinting (LBB)

This method, as the name indicates, relies on the usage of a laser to produce droplets. It consists of three components, namely an energy-absorbing layer, a donor ribbon, and a bioink layer. A laser pulse is absorbed by an energy-absorbing layer generating high pressure in the donor ribbon leading to the creation of a bubble.[23,24] This bubble pushes the bioink layer, causing a droplet to form, which is then deposited on the substrate (Figure 4).[23] Laser-based direct writing (LDW) is the most common laser-based bioprinting method since it can maintain high cell viability while creating precise patterns. The main advantage of LBB is printing relatively high-viscosity bioinks with a high level of resolution thanks to its nozzle-free printing process.[25,26] However, like every other bioprinting methods, LBB has some disadvantages, such as some degree of cell damage that may occur thanks to the increasing heat originated by the laser energy.[25,26] Additionally, prolonged fabrication times, the need for photo-crosslinkable materials, and the complexity of this technique are also seen as the main disadvantages.[24]

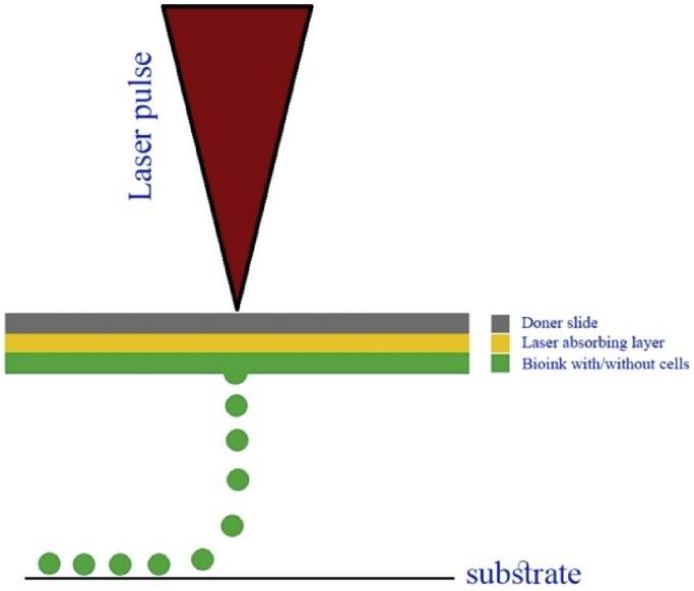

Figure 4 - Representation of laser-based bioprinting mechanism.

2.4. Photocuring-based bioprinting (PBB)

This method utilizes photosensitive polymers under controlled lighting.[12] It avoids disadvantages like nozzle plugging and shear stress compared to other 3D bioprinting approaches, also presenting higher resolution and printing speed.[12] This bioprinting method can be subdivided into stereolithography (SLA) and digital light processing (DLP).[12]

SLA relies on ultra-violet (UV) light to generate thin layers of solid material by polymerizing liquid resins. The first layer is created by solidifying the bioink solution upon exposure to UV light.[12,27] After the first layer is formed, the structure moves, allowing for the creation of new layers, which adhere to the previous ones, resulting in a 3D structure. This method does not depend on a nozzle, so as mentioned in other nozzle-free methods, it has high cell viability (exceeding 95% in this case), also achieving high print repeat accuracy, allowing the control over the porosity, resolution, and mechanical properties of the final construct.[27] However, the high equipment cost and the complexity in the usage of this method are some of the disadvantages of it, such as the usage of UV light that can sometimes affect cell viability.[12]

In contrast to SLA, which solidifies a layer point-by-point, DLP can solidify a complete layer at once since it uses a projector as a light source (Figure 5). This significantly reduces the printing time since no matter how complex the final product might be, the printing time

of each layer remains the same.[28] Also, the structures produced by this bioprinting method are smoother than the structures made by inkjet-bioprinting and extrusion-based. [12,28]

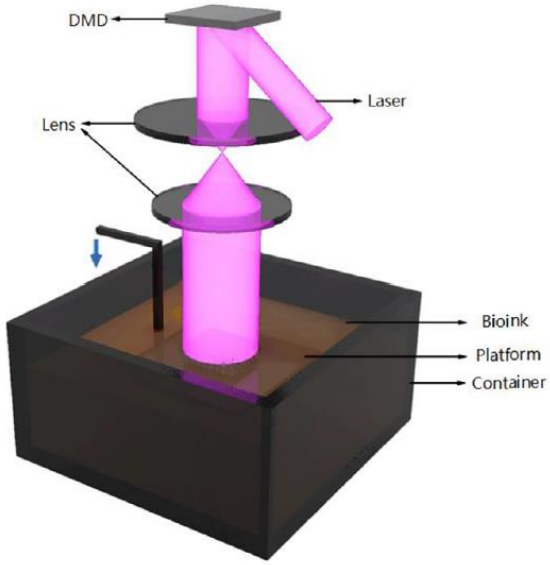

Figure 5 - Representation of DLP bioprinting principles. (Adapted from Zeming Gu. *et al.*, 2019)[12].

3. Bioinks

Bioinks represent one of the essential parts of the bioprinting process. The selection of the adequate bioink is made accordingly to specific parameters, such as the bioprinting method and the type of cells.[3]

Two major types of bioinks have been developed for 3D bioprinting applications, namely scaffold-based bioinks and scaffold-free bioinks.[29] Scaffold-based are the most common ones and are composed of cells and an exogenous material, as hydrogels and microcarriers, which will be used in the course of this work. On the other hand, for scaffold-free bioinks, cells are printed without the use of exogenous material in a process that mimics embryonic development.[3]

Bioinks must have specific characteristics, such as high printability, being insoluble in the physiological medium, having great mechanical stability, guarantee a suitable degradation rate, and being cytocompatible and non-immunogenic.[30] In the following section, we will discuss the different bioink materials, focusing on their characteristics and advantages/disadvantages.[3,31]

3.1. Scaffold-free bioink materials

Scaffold-free bioinks are cell suspensions rising in popularity for the fabrication of tissues or organs since they mimic embryonic development through cellular self-assembly mechanisms.[32] These cells are bound by cadherin molecules and by producing their own ECM. These cadherin molecules promote intercellular adhesion, enable signal transduction and increase integrin expression.[3] Integrin will be later responsible for the cytoskeleton adhesion to the ECM, subsequently resulting in a fully developed tissue. Scaffold-free bioinks can be divided into three different types: tissue spheroids, cell pellets, and tissue strands.[32]

3.1.1. Tissue spheroids

Tissue spheroids are densely packed aggregates of living cells that can only be bioprinted by EBB.[3,32] Tissue spheroids are typically formed following a three-step procedure. Firstly, cells are compacted and fused, generating high-density aggregates of cellular spheroids. The second step consists of the spheroid's proliferation, and lastly, there is their aggregation, resulting in multicellular aggregates which can be used as bioinks for 3D bioprinting of tissue constructs.[32]

There are various techniques for tissue spheroids' fabrication. The most popular one is casting some cells into non-adhesive hydrogels, followed by their culture in microwells. Whenever these cells are seeded in the microwells, they contact each other resulting in cadherin production and cell aggregation.[3] The hanging drop method is another well-known technique for the production of tissue spheroids.[32] In this case, the cells are dispensed in a culture plate, turned upside down. Due to the surface tension and gravitational force, cell spheroids begin to form at the bottom of the droplets (Figure 6. A).[32]

During the bioprinting process of tissue spheroids, they can be loaded into a dispensing tip. Due to the pressure applied on this tip, the tissue spheroids are extruded one by one generating a precise conformation.[3] Spheroids are not printed alone; typically, they are printed alongside a mould which can be a hydrogel (Figure 6. B), which supports the fusion and maturation of the spheroids. Later the spheroids will merge to create a more extensive scale tissue that can be easily separated from the mould.[3]

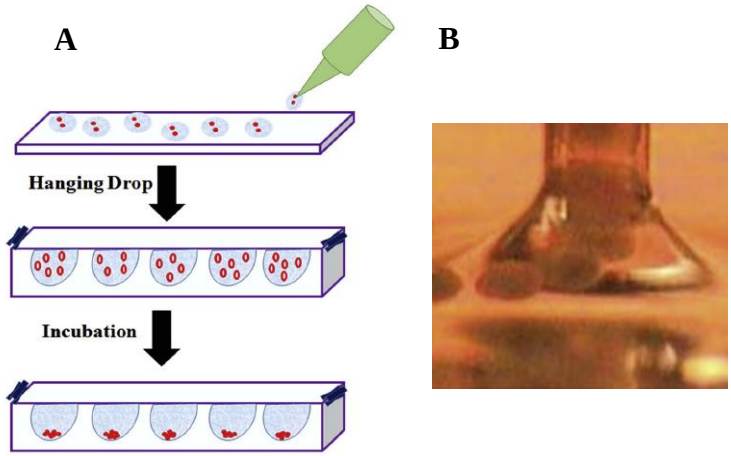

Figure 6 - (A) Schematic representation of the hanging drop method for the production of tissue spheroids; (B) Bioprinting of tissue spheroids (Adapted from Monika H. *et al.* (2017))[3].

3.1.2. Cell pellets

Cell pellets are increasingly becoming a standard method to prepare bioinks for scaffold-free tissue fabrication.[3] This technique uses both centrifugal or gravitational forces to concentrate cells at the end of a mould, which can be a conical tube or a micropipette where intercellular interactions will occur (Figure 7. A) without the need for sophisticated systems.[3,33] Even though this method is practical, it generates aggregates with limited oxygen and medium circulation, which may decrease cell viability.[33] These bioinks can only be used with EBB. In Figure 7. B cell pellets are being extruded into a supporting agarose mould, which facilitates the aggregation of the cells.[3]

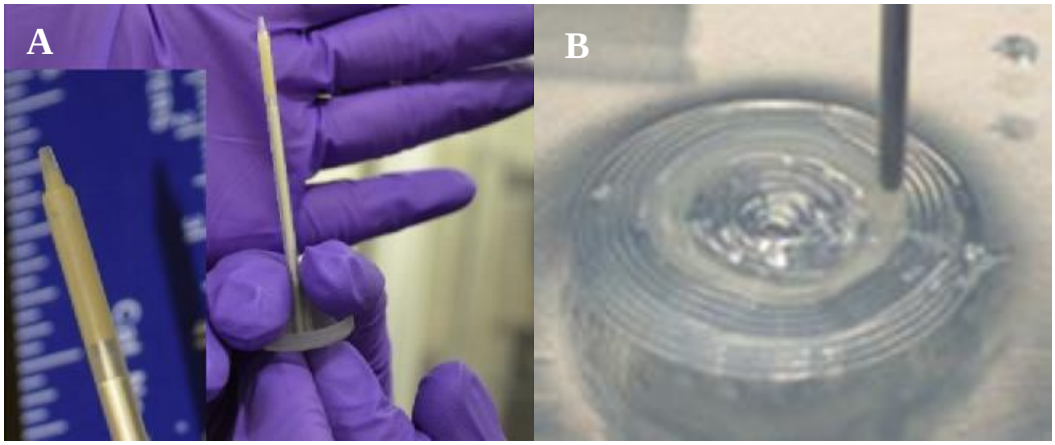

Figure 7 - (A) Cell pellet in a nozzle tip; (B) Printed cell pellet inside an agarose mould mimicking an aortic vessel (Adapted from Monika H. *et al.* (2017))[3].

3.1.3. Tissue strands

In the case of tissue strands, the cell aggregation occurs after packing and injecting previously extracted cell pellets into hollow alginate tubes with high mechanical properties and well-defined permeability. These cells then grow without attaching to the alginate luminal surface, resulting in cylindrical strands (Figure 8. A).[32] After the cells aggregate into a neo-tissue, the alginate tubes are dissolved using a solution that reverts the cross-linking, resulting in the final tissue strand (Figure 8. B).[3] This tissue strand is later placed into a bioprinter head being mechanically extruded. (Figure 8. C)[3] In order to assure an appropriate bioprinting process, the tissue strands need to be matured to avoid the formation of undesired shapes and disintegration during the bioprinting process.[3] This method offers high cell viability since it produces a favourable and safe environment for the cells.[3] For example, this technique makes tissues with a high degree of ECM deposition when creating cartilage tissues, which is fundamental for producing viable tissues.[34] However, this procedure requires a large expend of cells, making it a more laborious and costly method.[34]

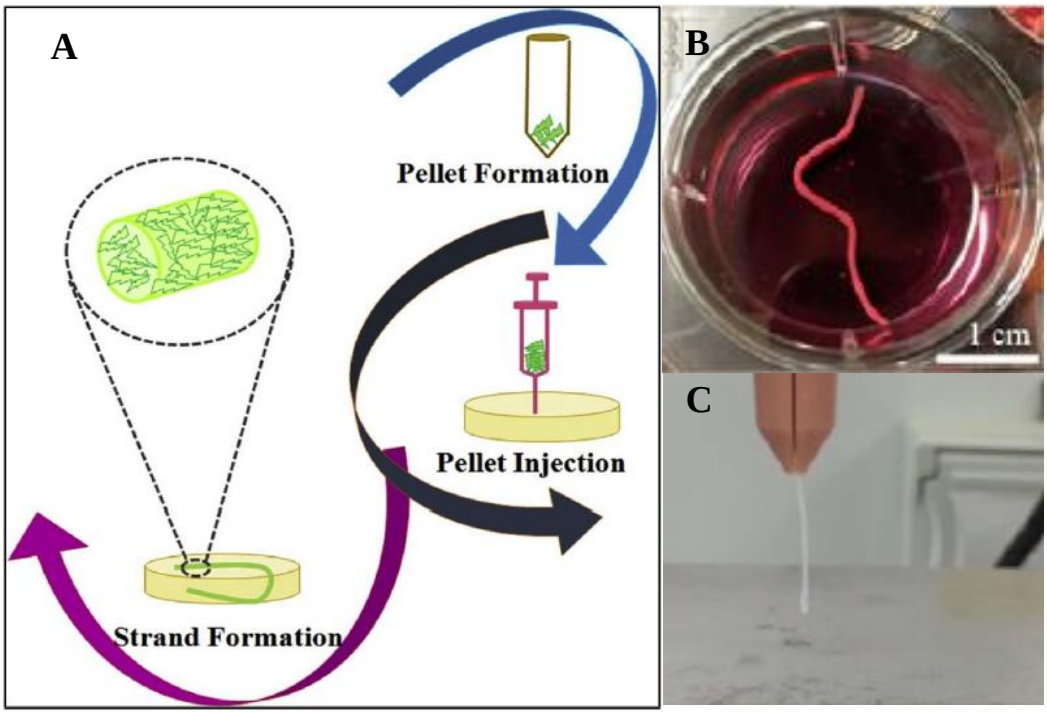

Figure 8 - (A) Schematic representation of tissue strands formation; (B) Tissue strand made of fibroblasts; (C) Long tissue strand (8cm long) during extrusion (Adapted from Monika H. *et al.* (2017))[3].

3.2. Scaffold-based bioink materials

A scaffold-based bioink, as previously mentioned, requires a supportive biomaterial in which the cells are laden, which is later degraded. Upon being biodegraded, the cells will then expand, forming a structured tissue.[3,31] Scaffold-based bioinks materials can be further divided into hydrogels, decellularized matrix components and microcarriers.

3.2.1. Hydrogels

Hydrogels are cross-linked polymeric networks capable of absorbing and retaining large quantities of water.[3] This high water content allows to obtain high biocompatible scaffolds due to their high hydrophilicity.[3,35] As previously mentioned, hydrogels are produced by cross-linking, which can be chemical or physical cross-linking.[36–38] The chemical cross-linking regularly involves free radical polymerization and enzymatic induced cross-linking as well as Diels-Alder "click" reactions, Michael type-additions and Schiff base formations.[39,40] This type of cross-linking is mainly based on the formation of covalent bonds, which are irreversible. Covalent cross-linking ends up giving firmness to the 3D network, although these confines cells, making them unable to vascularize within engineered tissues and proliferate.[38] On the contrary, physical cross-linking processes, such as reversible intermolecular interactions (ionic/electrostatic interaction), hydrogen bonds, hydrophobic/hydrophilic interactions, etc.[39,40] lack exogenous agents and chemical interactions, thus being typically non-cytotoxic and displaying a reversible network character.[3,38,41] Naturally-derived hydrogels are mainly formed by physical cross-linking processes.

In tissue engineering, hydrogels can mimic a native 3D environment, being therefore, more often used to produce cell-laden bioinks.[3] They can be classified into two main groups: naturally-derived and synthetically-derived hydrogels.[3] This division is made accordingly to the nature of the polymers used to produce them. Naturally-derived hydrogels can be further categorized into protein-based and polysaccharide-based (Figure 9).[36]

Naturally-derived hydrogels, such as those based on gelatin, chitosan, and alginate (Figure 9), are generally weak in terms of mechanical properties, have high biodegradability rates, high biocompatibility, high variability, and lack of customization.[3] In contrast, the synthetically-derived hydrogels, such as Pluronic® or poly(ethylene glycol) (PEG) based ones (Figure 9), have good mechanical properties and can be customized, although some of

them may lack biocompatibility.[3] To surpass these issues, from both naturally-derived and synthetically-derived hydrogels, the creation of hybrid hydrogels by combining synthetic and natural polymers has been rising in popularity.[37,38] Hybrid hydrogels can overcome both the biocompatibility issue from the synthetically-derived hydrogels and the lack of tunability from the naturally-derived hydrogels since they result from the cross-linking between natural and synthetic polymers.[3,38] Thanks to the customization of these hybrid hydrogels, it is possible to achieve higher biocompatibilities and tunable mechanical properties such as hydrogel's distortion prevention.[42]

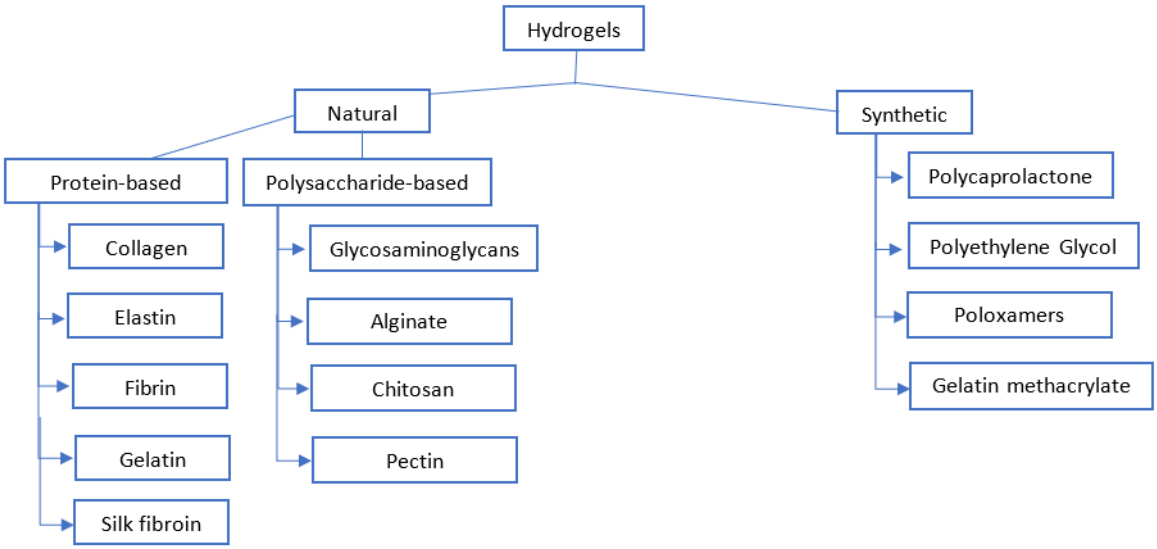

Figure 9 - Schematic representation of the classification of hydrogels and some of the most used polymers to produce them.

In Figure 10, there are some examples of bioprinted hydrogels from both natural and synthetic based polymers.

Another strategy to improve the mechanical properties of hydrogels is the use of reinforcing fibers.[42] Cellulose, spider silk, and collagen are some of the natural fibers used in 3D-bioprinting, conferring the mechanical resistances that the hydrogel lacks while showing high biocompatibility, abundance and strength.[42] However, reinforcing fibers can also be synthetic, such as glass, ceramic fibers, or even polymers (*i.e.*, polyamides and polyesters). These can be altered in terms of molecular structure or even characteristics to fit any specific application's needs.[42]

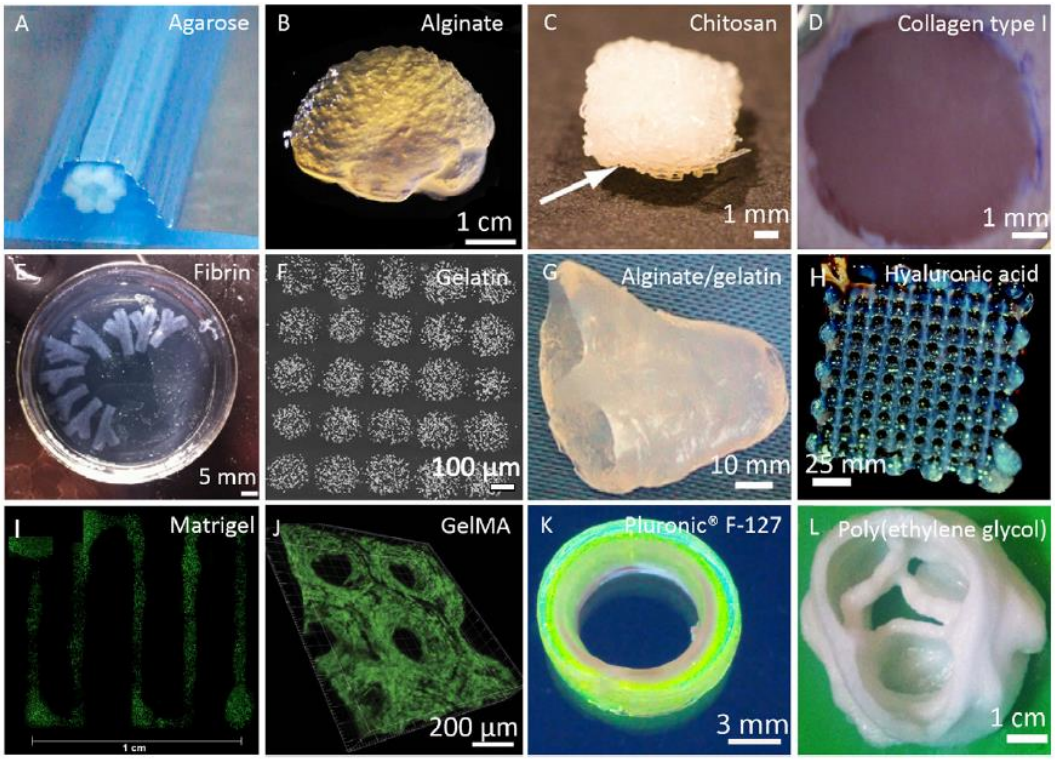

Figure 10 - Bioprinted hydrogels: (A) agarose filaments; (B) 3D printed alginate in brain shape with anatomical features; (C) chitosan scaffold after 4 weeks of culture; (D) collagen type I construct for skin tissue regeneration; (E) bioprinted fibrin into 3D tubular scaffolds; (F) gelatin bioprinted by laser direct-write technique resulted in precise deposition of cells; (G) 3D bioprinted 'half-heart' scaffold using an alginate/gelatin bioink; (H) bioprinted hyaluronic acid; (I) 3D bioprinted hepatic carcinoma cell-laden Matrigel graft; (J) a 3D confocal image of cells in a GelMA (gelatin methacrylate) scaffold fabricated by LBB; (K) bioprinted Pluronic® F- 127 fluorescent tube; (L) PEG hydrogel bioprinted into aortic valve construct. (Adapted from Monika H. et al. (2017)[3].

Cellulose fibers are commonly used since they are the most abundant organic macromolecule on earth.[43] To form hydrogels, cellulose is usually modified, enhancing its properties and its cross-linking capacity.[44] However, cellulose has been used more frequently as a reinforcement element due to the emergence of nanometric forms of this polymer, such as nanofibrillated cellulose, bacterial cellulose and cellulose nanocrystals.[45–47] Nanocellulose has been widely researched and used in medical applications for being non-toxic, non-carcinogenic and mainly biocompatible.[44] For example, Markstedt *et al.* developed a bioink of alginate, which was reinforced with nanocellulose fibrils and laden with human chondrocytes.[48] The resultant bioink presented high biocompatibility, fidelity and stability with optimal mechanical properties for 3D bioprinting[48] (Figure 11).

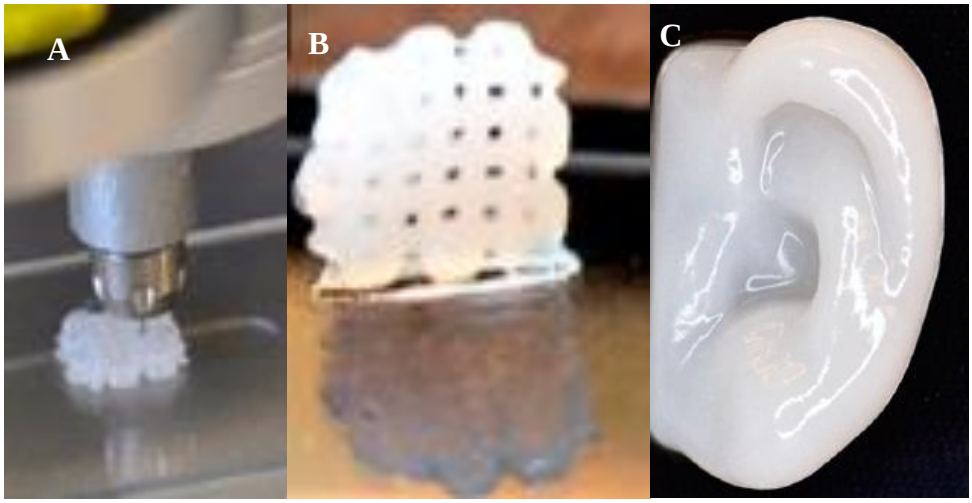

Figure 11 - (A) Bioprinting of alginate+nanofibrillated cellulose bioink; (B) alginate+nanofibrillated cellulose 3D printed grids; (C) 3D printed human ear. (Adapted from Markstedt et al., 2015)[48].

3.2.2. Decellularized matrix components

The extracellular matrix (ECM) is a 3D structure secreted by the cell itself, responsible for proliferation, signalling, tissue development, and cell attachment.[3] The decellularized extracellular matrix (dECM) is obtained by removing cellular material by chemical, enzymatic, or physical processes.[3] After decellularization, the obtained dECM can be used to produce bioinks.[3]

The decellularization processes tend to be time-consuming to guarantee complete decellularization while minimizing ECM loss and damage.[49] The chemical and enzymatic processes are the most widely used.[50] Detergents are usually used as chemical agents since they can solubilize and dissociate the inner structure of the cell's membranes, being Triton X-100 and sodium dodecyl sulfate (SDS) the most common ones.[49] These detergents are valuable and effective to eliminate cells from various tissues, mainly tissues which have high protein levels.[49] Triton X-100 mainly targets lipid-lipid and lipid-protein interactions, while SDS tends to denature proteins, solubilizing both external and nuclear membranes. As for the enzymatic agents, trypsin is the most commonly used enzyme for decellularization.[49] This enzyme targets amino acids like arginine and lysine and can even destroy cell-matrix interactions when combined with ethylenediaminetetraacetic acid (EDTA), a chemical agent.[49] However, these processes can induce cytotoxicity.[50] Thanks to this, physical process has started to rise as an alternative to the chemical and enzymatic counterparts. Physical

techniques as perfusion can sometimes be used to reach all tissue areas better. However, these techniques are not enough to decellularize the tissue. To improve decellularization, sometimes both methods can be combined, gathering both chemical and physical processes' advantages, creating a dECM that is more suited for a specific application.[49] After decellularization, DNA is quantified to determine if the matrix is fully decellularized. If the percentage of decellularization is around 98%, it means it was successful.[51] The dECM presents the ideal mechanical properties and micro-environment for cell proliferation and differentiation.[3,49] In a recent study, after in-vivo implantation of dECMs with stem cells, there were no signs of cytotoxicity or inflammation, which is one of this bioink's advantages.[52]

In Figure 12, there is an example of a tissue construct that was printed with dECM, and also a tissue construct that was printed with dECM in combination with a PCL framework.[51]

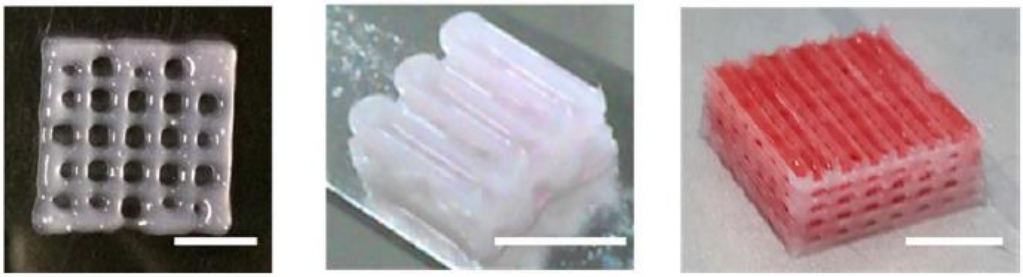

Figure 12 - Tissue constructs bioprinted with dECM bioinks: (A) Heart tissue construct was printed with only heart dECM (hdECM); (B) Cartilage tissues printed with cartilage dECM (cdECM) in combination with PCL framework; (C) Adipose tissue printed with adipose dECM (adECM) in combination with PCL framework (scale bar, 5mm). (Adapted from Pati F. *et al*., 2014)[51].

3.2.3. Microcarriers

Microcarriers are supportive structures that provide a large surface area for cell growth and expansion because of their interconnected pores in a spherical architecture, representing a space-saving and cost-effective culture system.[3,53] Microcarriers, as hydrogels, can be made either of natural (e.g. cellulose, gelatin, collagen and dextran) or synthetic (e.g., glass, thermoplastics) materials.[53] The synthetic derived microcarriers suffer from poor cell adhesion, which does not happen with the natural derived ones.[54]

Microcarriers can be further divided into two major categories, solid or liquid, considering the substance the cell grows on.[54] Solid microcarriers protect the cells against external stresses since they provide internal spaces for cells to attach. However, these microcarriers lack oxygen/nutrient transportation systems, and the accumulation of toxic metabolites inside their structure typically occurs.[54] To avoid some of these issues, liquid microcarriers were created based on a liquid/liquid interface consisting of a growth medium and a hydrophilic liquid.[54] It is possible to harvest cells using enzyme-free methods using perfluorocarbon and growth medium interface, leading to the diminishment of cell damage. More advanced liquid interfaces can be created, diminishing the disadvantages and improving the customization of these microcarriers.[54]

Microcarriers supporting role has been rising in attention since it can improve the bioprinting viability and success. These structures can be loaded with bioactive compounds that will control their spatial and temporal distribution, becoming a much more precise method that can guide the development and differentiation of the cell to a specific goal, maximizing cell-cell interactions[3,54]

Microcarriers embedded in hydrogels have revealed great potential for 3D-bioprinting. Microcarriers can be used as reinforcement units in bioinks, giving the produced inks shear-thinning properties optimal for bioprinting while also giving loaded cells structural support thanks to the hydrogels' matrices.[55–57]

For example, Levato *et al.*[55] tried reinforcing gelatin methacrylate (GelMA)-based hydrogels with poly(lactic acid) microcarriers. The results showed that the microcarriers acted as a mechanical reinforcement to the hydrogel matrix without compromising the printability.[55] Additionally, when loaded with Mesenchymal stromal cells, the microcarriers ended up supporting bone matrix deposition, revealing high interest for the 3D-bioprinting of bone tissue.[55] Figure 13 shows a microcarrier laden with cells from a study that aimed to develop coherent 3D models of epithelia (Figure 13.A) as well as an immunofluorescence image of the printed construct of Levato *et al*.[55] (Figura13.B).

As mentioned previously, cellulose nanometric forms have already demonstrated high potential in 3D-bioprinting. In this way, in this study, cellulose acetate microparticles were loaded into an alginate hydrogel, aiming to reinforce the alginate hydrogel and give the future loaded cells higher structural support.

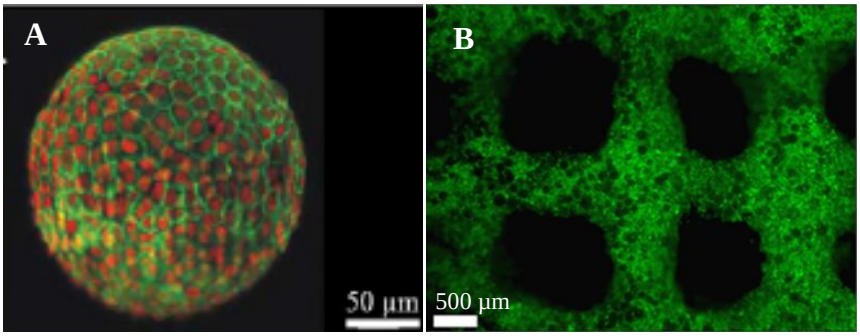

Figure 13 – Microcarriers for bioprinting. (A) A fluorescence image of a cell-laden microcarrier, where cell surface and nucleus were stained in green and red, respectively (Adapted from Monika H. *et al.* (2017))[3]; (B) Immunofluorescence staining for actin cytoskeleton of bioprinted microcarriers with encapsulated cells loaded in a gelatin methacrylate (GelMA) hydrogel matrix. (Adapted from Levato *et al.* (2014))[55].

4. Materials and Methods

In this chapter, the chemicals and materials used, and the methodologies employed to produce the cellulose acetate microparticles and the corresponding bioinks will be described. The characterization techniques employed to characterize all materials will be also presented.

4.1. Chemicals and materials

Cellulose diacetate membranes were obtained from FILTER-LAB (Barcelona, Spain). Alginic acid sodium salt from brown algae (low viscosity) was acquired from Sigma-Aldrich. Calcium chloride anhydrous (96%) was supplied by Carlo Erba Reagents (Barcelona, Spain). Dulbecco's Modified Eagle's Medium (DMEM) was obtained from PAN-Biotech (Germany). Fetal bovine serum (FBS), phosphate buffer solution (PBS, pH 7.4), L-glutamine, penicillin/streptomycin and fungizone were obtained from Gibco® (Life Technologies, Carlsbad, CA, USA). L-Glutamine solution 200 mM and Penicillin/Streptomycin solution were obtained from Grisp (Porto, Portugal). Trypsin-EDTA solution 10x (0.5% trypsin, 0.2% EDTA) was obtained from SIGMA-Aldrich. 3-(4,5-dimethylthiazol-2-yl)-2,5-diphenyltetrazolium bromide (MTT, 98%) and dimethyl sulfoxide (DMSO, ≥99.9%) were obtained from SIGMA-Aldrich. Other solvents were of laboratory grade.

4.2. Production and characterization of cellulose acetate microparticles

4.2.1. Production of the cellulose acetate microparticles

To prepare the cellulose acetate microparticles, 79 mg of cellulose acetate were dissolved in 20 mL of acetone under magnetic stirring at 500 rpm. Then, distilled water (15 mL) was added drop-wise using a syringe with a 0.45 mm needle gauge under continuous stirring at 500 rpm to regenerate the CA microparticles by the water-on-polymer method.[58]

Afterwards, the resulting suspension was heated in an oil bath at 65-75 ºC for 60 minutes, centrifuged at 6000 rpm for 15 min and the supernatant carefully removed. The CA microparticles were then resuspended in distilled water and centrifuged again, repeating this process two times. 15 mL of CA microparticles suspension is obtained following this procedure with a concentration of 1.33 mg/mL. The actual concentration of the suspension

was determined by calculating the dry weight of 3 ml of suspension. After obtaining the value of the actual concentration, the yield of the microparticles' production process was determined through the following formula:

$$\eta = \frac{[Real\ concentration]}{[Expected\ concentration]} x100$$

4.2.2. Fourier transform infrared-attenuated total reflection (FTIR-ATR) spectroscopy

The structure analysis of the freeze-dried cellulose acetate microparticles and of the initial cellulose acetate (for comparison) was carried out by Fourier transform infrared spectroscopy using a Perkin Elmer FT-IR System Spectrum BX spectrophotometer (Perkin-Elmer, Waltham, MA, USA), equipped with a single horizontal Golden Gate ATR cell. The analysis was carried out in the range of 500 to 4000 cm^{-1} with an interval of 1 cm^{-1}.

4.2.3. Scanning transmission electron microscopy (STEM)

To carry out the STEM analysis, a dilution of the cellulose acetate microparticles suspension was performed. For this, 40 µL of the obtained cellulose acetate microparticles suspension was diluted in 960 µL of ultrapure water (MilliQ). A single droplet of the diluted solution was deposited on a copper (Cu) grid and left to dry overnight.

STEM analysis was performed at two magnifications (60000× and 10000×) to evaluate the microparticles' morphology with a SEM Hitachi SU-70 equipment (Hitachi High-Technologies Corporation, Tokyo, Japan) operated at 4 kV. The average size of the microparticles was determined by calculating the size of a total of 100 microparticles with the ImageJ software (National Institute of Health, USA).

4.2.4. *In vitro* cytotoxicity assays

The *in vitro* cytotoxicity of the cellulose acetate microparticles was evaluated in a human keratinocytes cell line (HaCaT cells) using the MTT assay.[48] HaCaT cells were grown in Dulbecco's Modified Eagle Medium (DMEM) culture medium supplemented with 10 % FBS, 2 mM L-glutamine, 100 U/mL penicillin, 10 µg/mL streptomycin and 250 µg/mL fungizone, at 37 ºC in a humidified atmosphere with 5 % CO_2. Cells were observed regularly

under an inverted phase-contrast Eclipse TS100 microscope (Nikon, Tokyo, Japan). Suspensions were prepared, sterilized by ultraviolet radiation (4 cycles of 20 min), and incubated with DMEM medium to obtain a concentration of 0.4 mg/mL, 2 mg/mL, and 4 mg/mL (for the assays corresponding to a microparticles concentration of 1%, 5% and 10% (m/m) respectively) at 37 ºC with 5 % CO_2 for 24 h to prepare the extracts.

Cells were seeded (60000 cells/mL for 24 h) in 96-well plates and incubated in the culture medium for 24 h to promote adhesion. Next, the cell culture medium was removed, and 100 µL of each extract was added to the wells and cells were again incubated for 24h. As a positive control, HaCaT cells were incubated with DMEM medium and treated the same way as the specimens. After the incubation time, 50 µL of MTT (1 mg/mL) in PBS was added to each well and incubated for 4 h at 37 ºC and 5 % CO_2. After that, the medium containing MTT was removed, and 150 µL of DMSO was added to each well. The plate was placed in a shaker for 2 h in the dark to promote the dissolution of the formazan crystals. The absorbance was measured with a BioTek Synergy HT plate reader (Synergy HT Multi-Mode, BioTeK, Winooski, VT, USA) at 570 nm. Cell viability was determined with respect to the control cells:

$$Cell\ viability\ (\%) = \left[\frac{Absorvance(sample) - Absorvance\ (DMSO)}{Absorvance\ (control) - Absorvance\ (DMSO)}\right] x100$$

4.3. Production and characterization of alginate-cellulose acetate microparticles based inks

4.3.1. Production of the alginate ink

An alginate solution (4% m/v) was prepared by dissolving 400 mg of alginate in 8 mL of ultrapure water (MilliQ) under magnetic stirring. Then, 2 mL of a 0.5% (m/v) calcium chloride solution were added to the alginate solution to promote its' crosslinking (alginate:calcium chloride = 4:1, weight ratio).

4.3.2. Production of the alginate-microparticles inks

To prepare the alginate-cellulose acetate microparticles based inks, 400 mg of alginate were mixed with variable volumes of microparticles suspension to achieve 1%, 5% and 10% (m/m) of microparticles with respect to the alginate mass. Ultrapure water was

added to the resulting alginate-microparticles suspensions achieving a final volume of 8 mL. The obtained suspensions were left to homogenize under magnetic stirring for one hour. Then, 2 mL of a 0.5% (m/v) $CaCl_2$ solution were added to the various alginate-microparticles suspensions (1%, 5% and 10%), with the help of a mechanical mixer, promoting the pre-crosslinking of the ink. The inks were placed in a falcon tube and let to rest overnight. Table 1 summarizes all solutions, suspensions and inks prepared in this study.

Table 1 - Identification and composition of the alginate solution, alginate-microparticles suspensions and inks prepared in this study.

Sample name	Alginate % (m/v)	Microparticles % (m/m)	Pre-crosslinker % (m/v)
Alginate solution			
Alg4%	4	-	-
Alginate-microparticles suspensions			
Alg4%+Microparticles 1%	4	1	-
Alg4%+Microparticles 5%	4	5	-
Alg4%+Microparticles 10%	4	10	-
Pre-crosslinked alginate solution			
Alg4%	4	-	0.5
Pre-crosslinked alginate-microparticles (Inks)			
Alg4%+Microparticles 1%	4	1	0.5
Alg4%+Microparticles 5%	4	5	0.5
Alg4%+Microparticles 10%	4	10	0.5

4.3.3. Production of the alginate-microparticles hydrogels

Fully cross-linked alginate-microparticles hydrogels were prepared to be used in rheology. These were produced by fully cross-linking the pre-crosslinked alginate solution (for comparison) and alginate-microparticles suspensions with a 0.5% (m/v) $CaCl_2$ solution.

4.3.4. Rheology

To investigate the rheological properties of the developed inks (and corresponding fully cross-linked hydrogels), rotational and oscillatory tests were performed in a Kinexus Pro Rheometer (Malvern Instruments Limited, Malvern, United Kingdom) with a cone-plate geometry (cone angle of 4º and diameter of 40 mm).

Rotational tests were performed for both alginate solution and alginate-microparticles suspension (before and after pre-crosslinking with a 0.5% (w/v) $CaCl_2$ solution) with a measurement gap of 1 mm and a shear rate applied from 0.1 to 100 s^{-1} (at least five samples per decade).

In order to determine the recovery rate of the alginate and alginate-microparticles based inks an oscillatory test consisting in 3-steps was carried out: (i) measurement of the storage modulus (G') in a relaxation stage, at 1 Pa for 1 min; (ii) measurement of the G' in a stress phase, at 100 Pa for 10 s; and (iii) a second measurement of the G' in a relaxation stage, at 1 Pa for 1min. The initial storage modulus was defined as the average storage modulus in the initial 1 min when the material was submitted to 1 Pa of shear stress. The recovered storage modulus was defined as the storage modulus measured 5 s after the shear stress reduced from 100 Pa back to 1 Pa. The percent recovery was defined as the recovered G' divided by the initial G' and multiplied by 100%.

The oscillatory stress sweep tests to determine the storage modulus (G') and the loss modulus (G") of the fully cross-linked hydrogels were performed at a frequency of 1 Hz, in a shear strain range from 0 to 100 %, and with a measurement gap of 2.5 mm (at 20 ºC).

All measurements were performed using a water lock to prevent dehydration of the samples and a Peltier module for temperature control. All analyses were carried out at 20 ºC.

4.3.5. 3D-printing studies

4.3.5.1. Optimization of the printing parameters: monolayer filaments

The printing tests were performed on a 3D-BIOPLOTTER from EnvisionTEC (Germany), represented in Figure 14.

The printing parameters, such as air pressure and printing speed, were determined by extrusion printing monolayer filaments with 10 cm length of the alginate ink. Initially, using a nozzle with 0.41 mm width, the speed was kept at 10 mm/s, and the air pressure varied from 0.5 bar to 2.0 bar. After that, to observe the relation between printing speed and strand width, the air pressure was fixed at the value which previously resulted in better resolution, and the printing head speed was varied from 5 to 25 mm/s. This process was repeated with nozzles with different widths (0.25 mm and 0.20 mm) and air pressure variations (1.5-3.5 bar and 2-5 bar, respectively).

Figure 14 - 3D Bioplotter® Developer Series (EnvisionTEC, Germany).

4.3.5.2. Optimization of the printing parameters: 3D constructs

Then, constructs with the pattern illustrated in Figure 15 (consisting of 10 layers with a space between filaments of 1.5 mm and 10 mm ×10mm dimensions) were printed to evaluate the ink's printability and resolution. Both the alginate and the alginate-microparticles inks (1%, 5% and 10% microparticles) were printed by extrusion printing with the conditions optimized before (air pressure: 1.5 or 2 bar, printing speed: 10 mm/s, temperature of the cartridge containing the ink: 18 ºC, the temperature of the platform = room temperature: ~25 ºC). The printed constructs were then fully cross-linked with a 0.5% (m/v) $CaCl_2$ solution.

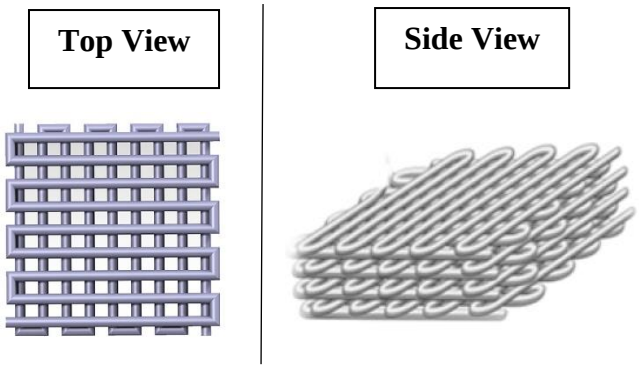

Figure 15 - Top and side representation of the printed construct template used in this study.

To improve the resolution of the printed constructs, additional printing studies maintaining the printing parameters previously defined (air pressure: 1.5 or 2 bar, printing speed: 8.5 or 10 mm/s, the temperature of the cartridge containing the ink: 18 ºC, the temperature of the platform = room temperature: ~25 ºC) and varying the space between filaments were carried out (1.5, 2.25, 3.0 mm). The number of scaffold layers was also varied (2, 4, or 6 layers). The printed samples were also cross-linked with a 0.5% (w/v) $CaCl_2$ solution.

4.3.6. Scanning electron microscopy (SEM) of the printed constructs

The presence of the CA microparticles on the fully cross-linked 3D-printed constructs, and their morphology, was observed through scanning electron microscopy (SEM). Alginate-microparticles (5% and 10%) 3D-printed constructs were freeze-dried for 24h prior to the analysis. The samples were coated with a carbon film and analyzed with a SEM Hitachi SU-70 equipment operated at 4kV and 3 different magnifications (30x, 500x and 1500x), obtaining surface micrographs. With the help of ImageJ software (National Institute of Health, USA), the space between filaments of the printed construct was determined and compared to the value set for the printing study.

5. Results and Discussion

The present work aimed to develop a novel biopolymeric microcarrier based bioink with improved mechanical properties and high cell viability taking advantage of the unique properties of cellulose acetate microparticles. In this perspective, cellulose acetate microparticles were produced and characterized in terms of their chemical structure (FTIR-ATR spectroscopy), morphology (STEM) and *in vitro* cytotoxicity. Then, alginate-microparticles suspensions with a concentration of alginate of 4% (m/v)[59] and variable concentrations of microparticles, namely 1%, 5% and 10% (m/m) (in respect to the alginate mass), were prepared. These suspensions were pre-crosslinked to adjust their viscosity and characterized in terms of their rheological behaviour. Finally, the 3D-printing process parameters, namely air pressure, printing speed, nozzle diameter, and space between filaments, were defined. The morphology of the printed constructs was also evaluated. A schematic representation of the procedure used in this study is presented in Figure 16.

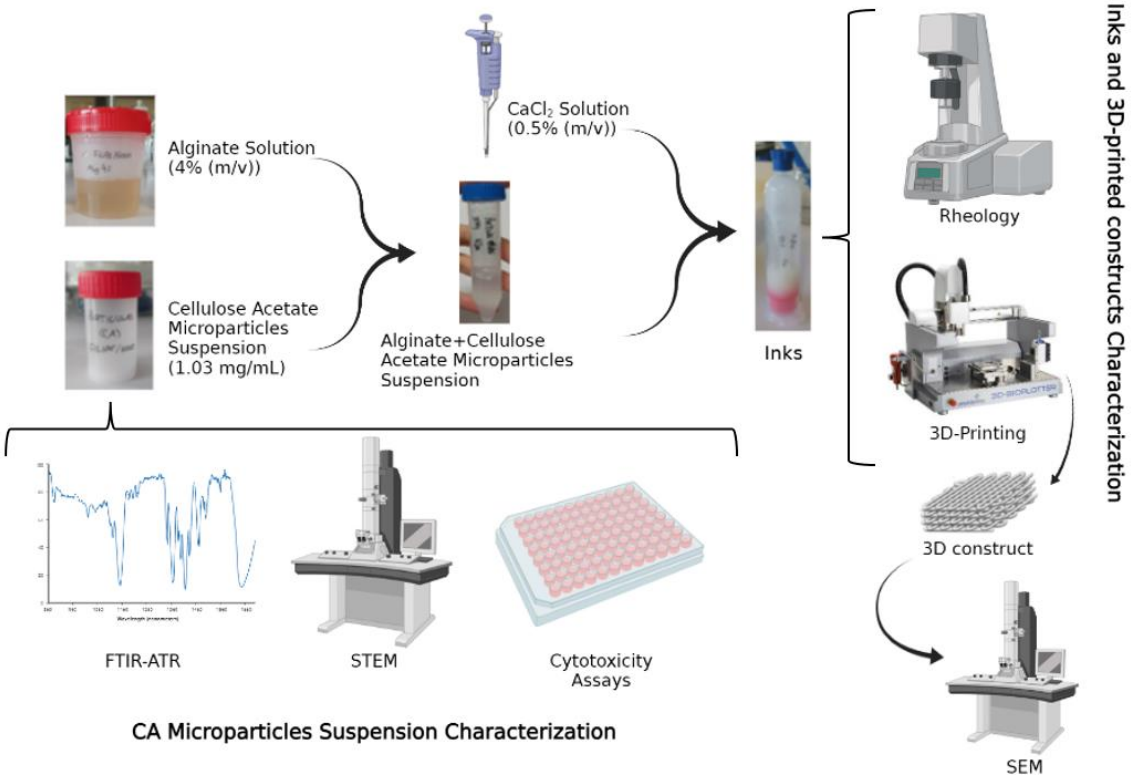

Figure 16 – Schematic representation of the procedure used to prepare and characterize the cellulose acetate microparticles suspensions, the inks, and the 3D printed constructs.

5.1. Production and characterization of cellulose acetate microparticles

Cellulose acetate microparticles were produced by the water-on-polymer method.[58] In this method, cellulose acetate is initially solubilized in acetone and later regenerated with the addition of distilled water drop-wise. When adding the distilled water, the solubility of cellulose acetate drastically falls, resulting in their precipitation and nucleation,[58,60] forming the cellulose acetate microparticles. Upon evaporating the remaining acetone, a suspension of microparticles is obtained. The yield of this process was 77.6%.

5.1.1. FTIR-ATR spectroscopy

The structural analysis of the microparticles was carried out by FTIR-ATR spectroscopy. The microparticles suspension was freeze-dried prior to the analysis. Figure 17 presents the FTIR spectra of the cellulose acetate microparticles and of the initial cellulose acetate (CA) for comparison.

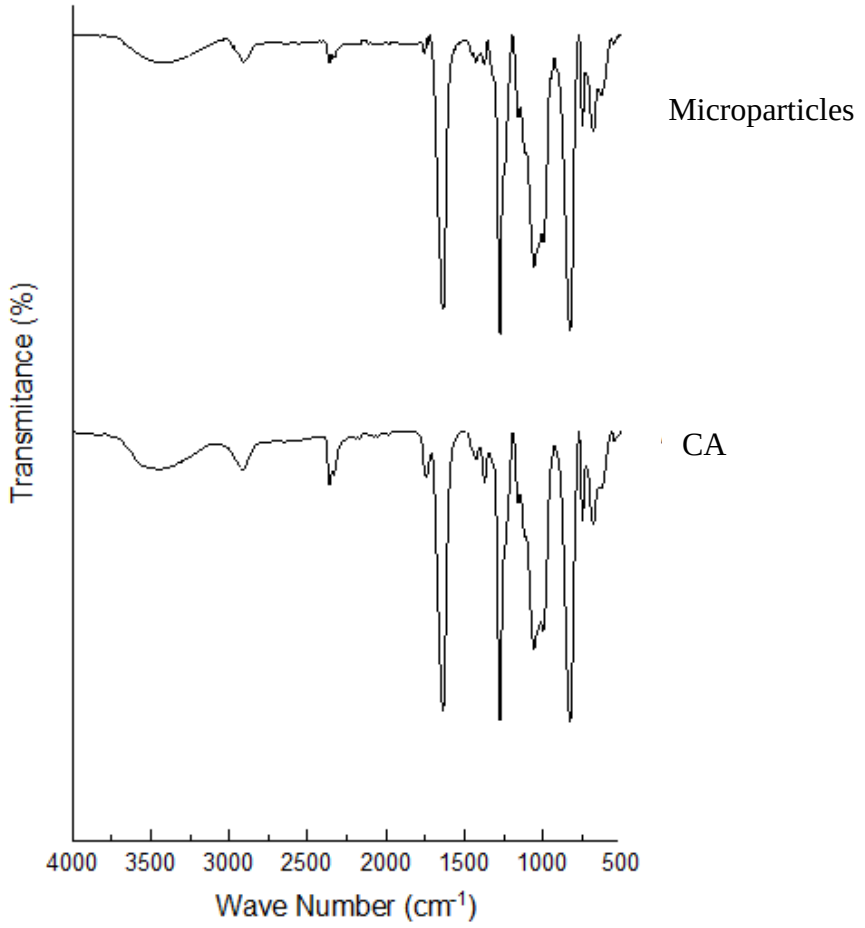

Figure 17 - FTIR-ATR spectra of the cellulose acetate (CA) and corresponding microparticles.

The spectrum of the initial cellulose acetate show several absorption peaks at 3399 cm^{-1} (-OH stretching), 2898 cm^{-1} (symmetric C-H stretching), 1634 cm^{-1} (C=O stretching), 1331 cm^{-1} (CH_2 wagging), and 1160 cm^{-1} (C-O-C stretching), which are characteristic of this cellulose derivative.[61–64]. When comparing the spectra of CA and CA microparticles (Figure 17), the absorption peaks are precisely the same, confirming that both microparticles and CA have the same chemical structure and, therefore, the methodology for the fabrication of the microparticles does not affect the chemical structure of CA.

5.1.2. Scanning transmission electron microscopy (STEM)

STEM analysis of the cellulose acetate microparticles suspension was carried out to analyze their morphological features and determine the average microparticles' size. This is an essential parameter for 3D-printing studies since it can lead to nozzle clogging.[65] Micrographs of the obtained microparticles are presented in Figure 18.

The microparticles revealed a spherical structure with an average size of 573.83±178.76 nm, which is in accordance with the average particle size of CA microparticles (100-1000nm).[66]

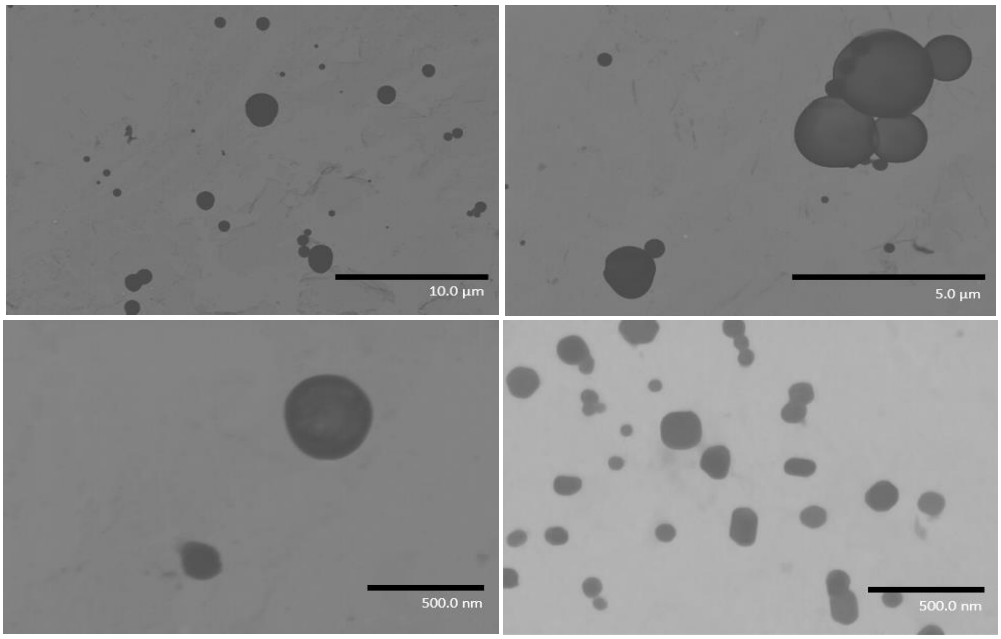

Figure 18 - STEM micrographs of the obtained CA microparticles.

5.1.3. *In vitro* cytotoxicity assays

The *in vitro* cytotoxicity of the CA microparticles was studied towards HaCaT cells to confirm their compatibility with living cells. The results of the cell viability for 24 h for these samples is shown in Figure 19.

The obtained results show that the microparticles suspension is non-cytotoxic towards HaCaT cells since the cell viability values were higher than 70% for every sample, confirming their potential to develop cell-laden bioinks.[48,67] Specifically, for the samples with 1% and 5% of microparticles, the cell viabilities were 99.7 ± 6% and 107 ± 6.3%, respectively. As for a microparticles concentration of 10%, the cell viability of HaCaT cells was 75±18%, thus also suggesting the non-cytotoxicity of the cellulose microparticles,[48,68]

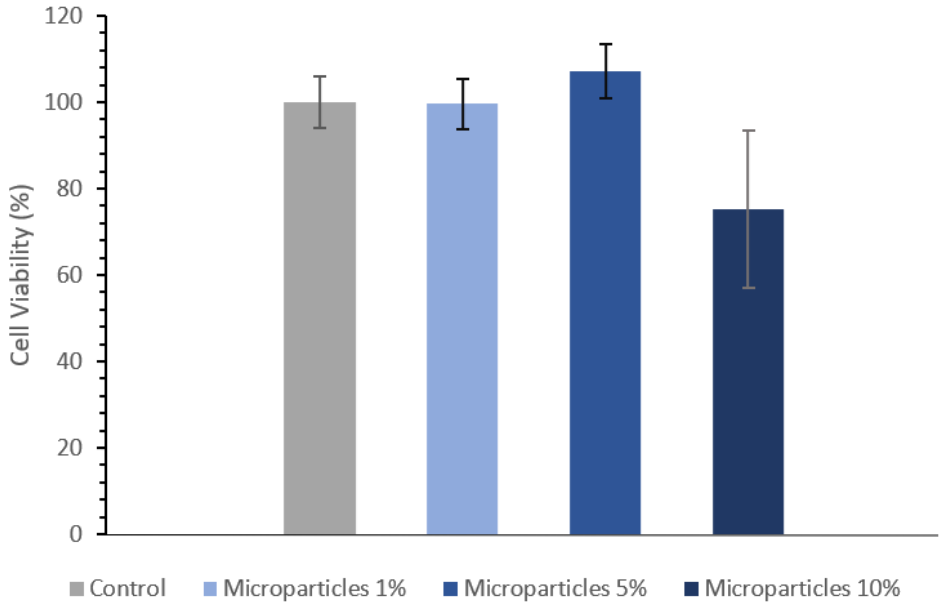

Figure 19 - HaCaT cells viability after exposure to different concentrations of cellulose acetate microparticles (1%, 5% and 10%) for 24 h.

5.2. Characterization of alginate-cellulose acetate microparticles based inks

Alginate-microparticles suspensions (and inks) with different CA microparticles concentrations (1%, 5% and 10% (m/m) in respect to the mass of alginate) were produced and characterized in terms of their rheological behaviour and the printing parameters optimized. The morphology of the printed constructs was also evaluated.

5.2.1. Rheological studies

The printability of hydrogel-based inks is highly dependent on their rheological properties.[69] Rheology aims to study how inks behave under certain stress and, therefore, predict how they will behave during a 3D-printing assay.[69,70] Thus, several rheological studies were carried out to characterize the responses of the different alginate-microparticles suspensions and corresponding inks and hydrogels to different shear rates and evaluate the effect of the addition of microparticles on the viscosity and shear stress of the alginate solution.

Both alginate solution (Alg4%) and the Alginate-microparticles suspensions (Alg4%+Microparticles1%, Alg4%+Microparticles5% and Alg4%+Microparticles10%) were characterized in terms of their viscosity and shear stress as a function of shear rate. These results are presented in Figure 20.

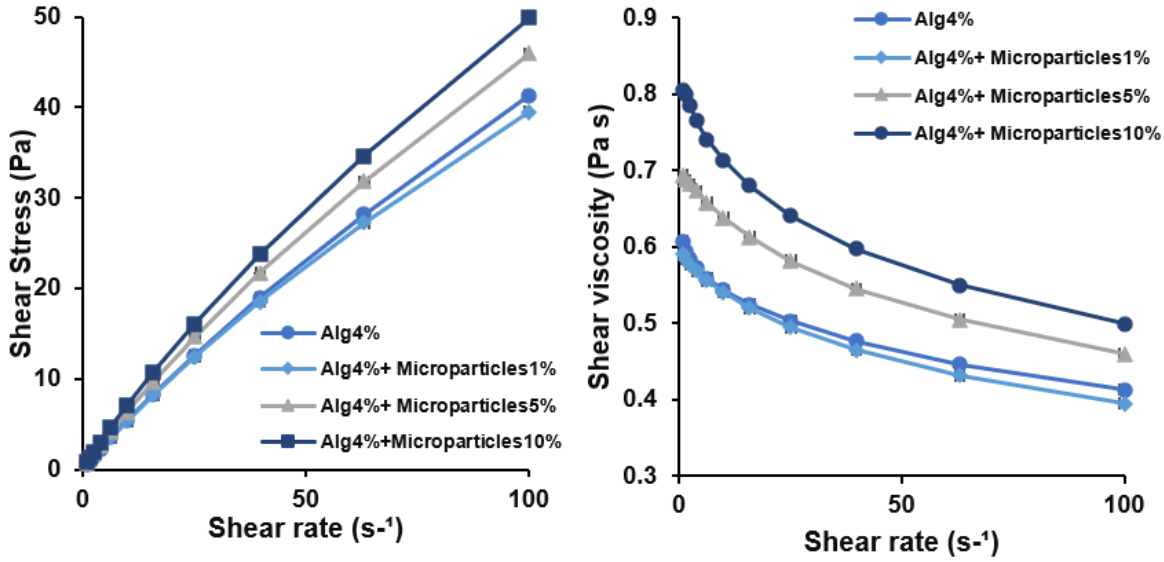

Figure 20 - Shear stress (left) and shear viscosity (right) as a function of shear rate for the alginate solution and alginate-microparticles suspensions with different CA microparticles concentrations.

As expected, the increase in the CA microparticles concentration generally leads to an increment of the shear viscosity and shear stress of the alginate solution.[69,71] This means that the microparticles are responsible for the increase in the viscosity of the various alginate-microparticles suspensions when compared to the alginate solution. A similar behaviour was reported by Heggset *et al.* [71], who studied the viscoelastic properties and printability of

cellulose nanofibrils (CNFs)-alginate inks and revealed that an increase in CNFs concentration leads to an increase in the ink's viscosity. In addition, the CA solution and all the suspensions present a shear-thinning behaviour, *i.e.*, increasing shear rates lead to a decrease in shear viscosity, typical of time-independent *non-Newtonian* fluids.[69,72]

Then, pre-crosslinked (with a 0.5% (m/v) $CaCl_2$ solution) alginate solution and alginate-microparticles suspensions (inks) were submitted to the same rheological studies. The results of the shear viscosity and shear stress as a function of the shear rate of these samples are presented in Figure 21. As previously observed for the alginate solution and alginate-microparticles suspensions, an increase of the microparticles concentration also leads to an increment of the shear viscosity and shear stress of the alginate inks. Moreover, the values for both shear stress and shear viscosity of the pre-crosslinked samples (inks) are noticeably higher than those obtained for the alginate-microparticles suspensions.[69,73] However, the differences between the viscosities of the alginate-microparticles inks are not as significant as those observed for the corresponding suspensions prior to the pre-crosslinking process, meaning that the cross-linking is the step that most affects samples viscosity. This pre-treatment reveals to be helpful to tune the printing parameters since all samples have identical rheologic properties.

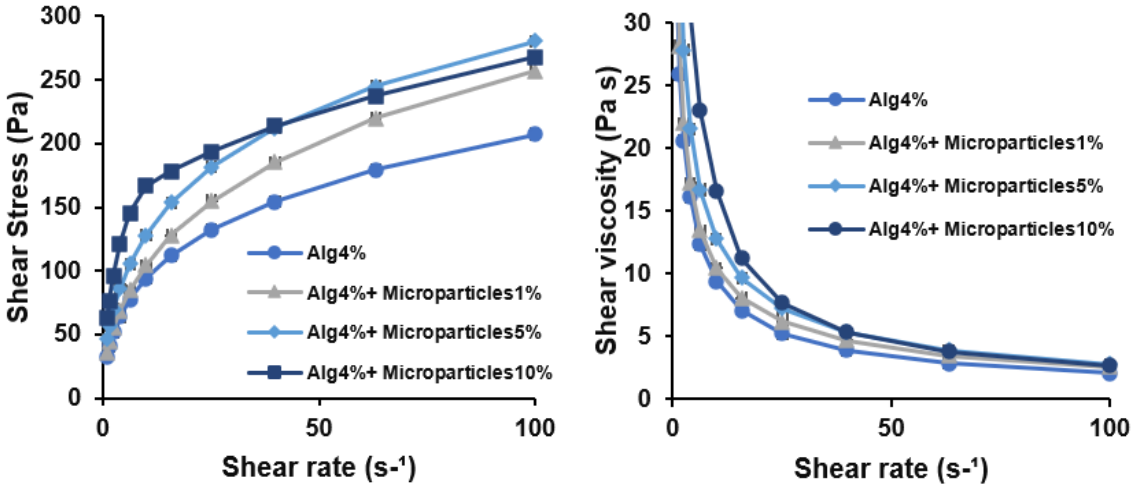

Figure 21 - Shear stress (left) and shear viscosity (right) as a function of the shear rate for pre-crosslinked (with a 0.5% (w/v) CaCl2 solution) alginate solution and alginate-microparticles suspensions with different CA microparticles concentrations (inks).

The inks recovery rate, which shows how well the original mechanical properties are recovered after the printing process[74], was determined, and the values are presented in Figure 22. The recovery rates for the alginate-microparticles inks were 93.78±0.72%, 93.59±0.67% and 83.81±1.48% for 1%, 5% and 10% (w/w) microparticles, respectively. As for the alginate ink, the recovery rate was 88.28±0.94%. We followed the minimum threshold of 85% to be a reasonable starting point and guideline for novel bioinks entering the literature, as suggested in Kiyotake *et al.*[74]. In this way, we can conclude that the alginate and the alginate-microparticles inks are adequate for extrusion printing applications.

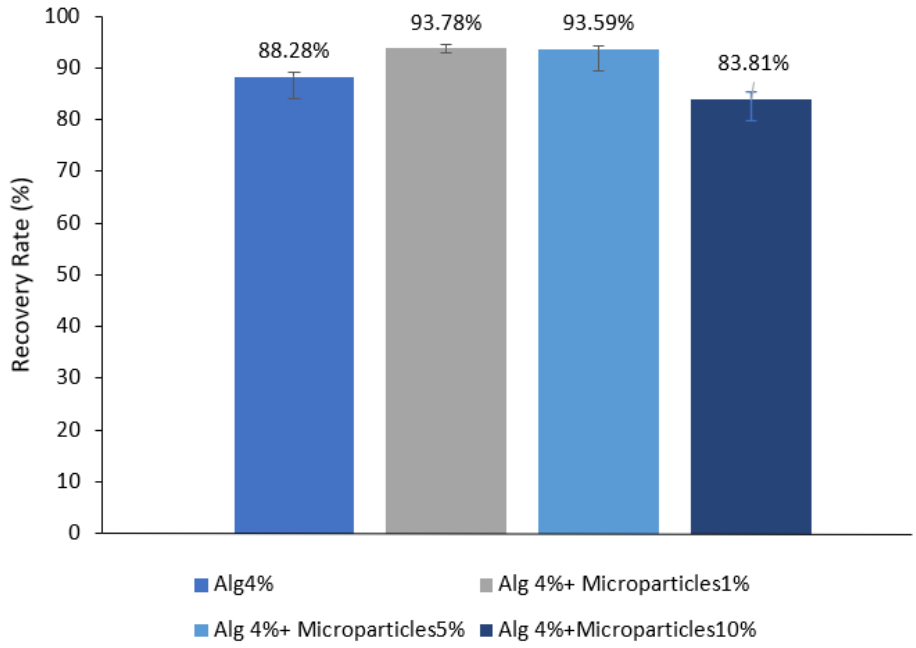

Figure 22 – Recovery rates of alginate and alginate-microparticles inks.

Then, alginate and alginate-microparticles hydrogels were prepared by fully cross-linking the alginate solution and alginate-microparticles suspensions with a 0.5% (m/v) $CaCl_2$ solution. These hydrogels were submitted to oscillatory rheology tests, thus obtaining the storage (or elastic) G' and the loss (or viscous) G" moduli. These parameters are essential to describe the viscoelasticity of the hydrogels.[69] The results for both G' and G" moduli are presented in Figure 23.

Regarding the results, the values obtained for the storage (G') modulus are significantly higher than those obtained for the loss (G") modulus (G'>G"), which indicate

that the hydrogels have a solid-like behaviour since G' represents the hydrogel firmness, and therefore are fully cross-linked.[69,75]

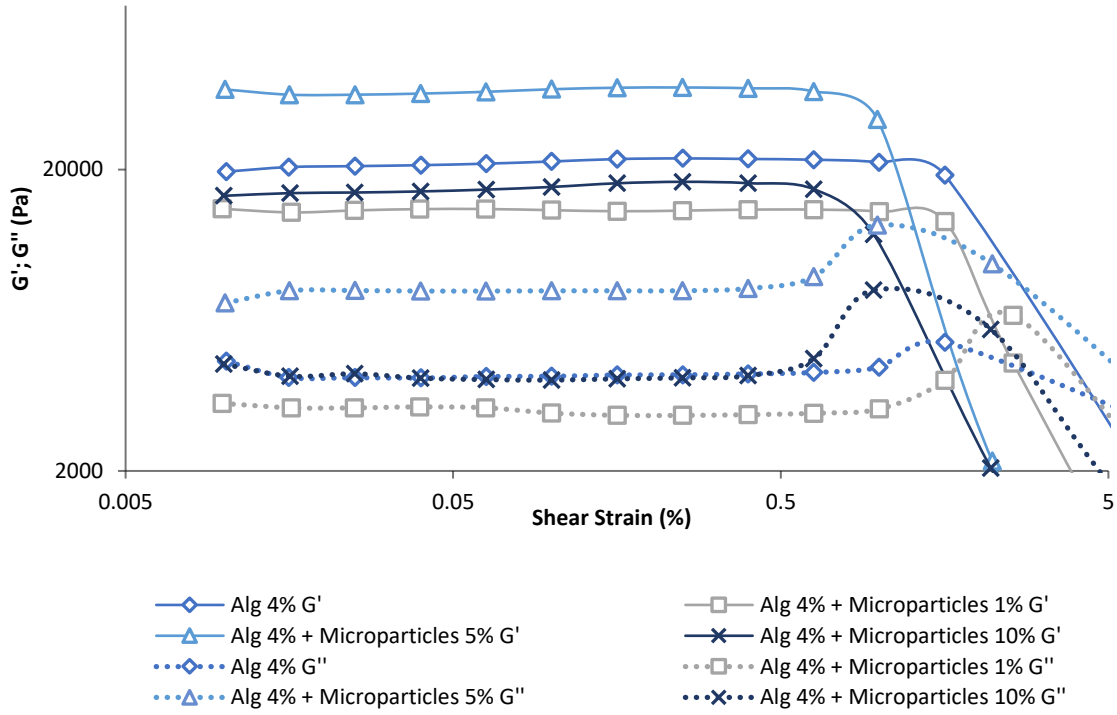

Figure 23 - Storage (G') and loss (G") moduli of alginate and alginate-microparticles hydrogels measured as a function of shear strain.

5.2.2. Optimization of the 3D-printing parameters

The printing parameters, namely nozzle width, printing speed and air pressure, were optimized by printing ink filaments using different nozzle widths and varying air pressure applied and printing speed. These tests were performed for the alginate ink (pre-crosslinked alginate solution) since the pre-crosslinked alginate-microparticles suspensions and the pre-crosslinked alginate solution had similar viscosities as referred above. Firstly, the tests were performed with a nozzle width of 0.41 mm. For this test, the air pressure was varied with a constant printing speed of 10 mm/s. In this way, the air pressure that presented the best resolution was selected, being 0.9 bar. Then, for this pressure, the printing speed was varied from 5 to 25 mm/s. Figure 24 presents the results for the different tests for the nozzle width of 0.41 mm.

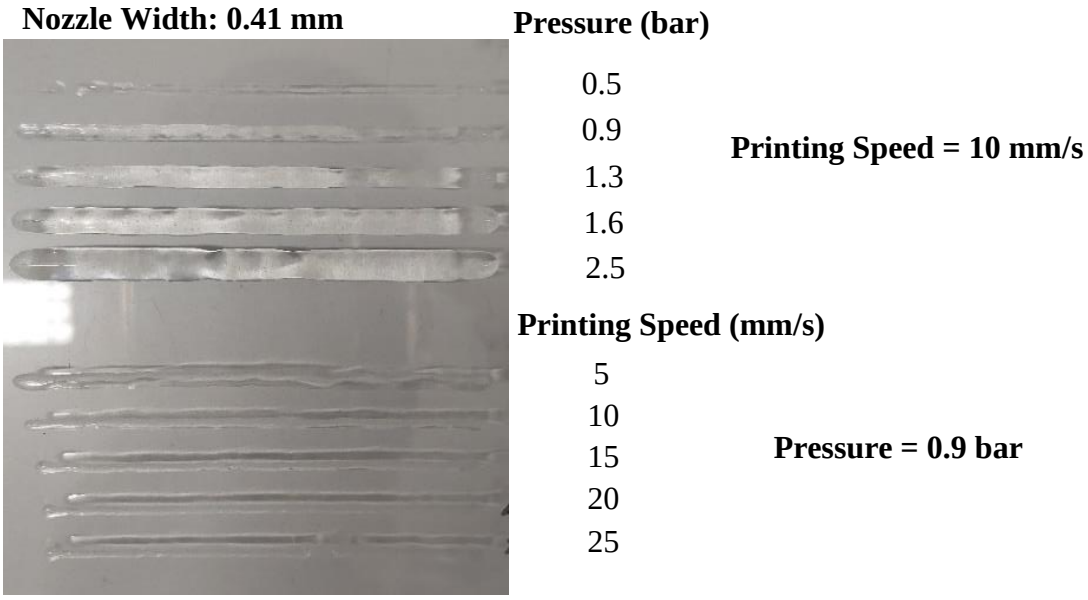

Figure 24 - Printing studies with the alginate 4% (w/v) ink using a nozzle with a width of 0.41 mm.

These results revealed that a large amount of ink is deposited for the 0.41 mm nozzle width, leading to filaments with a low resolution. Therefore, this width was discarded for these samples. To achieve higher resolution, a nozzle with 0.20 mm width was tested. Similarly, air pressure was varied, maintaining the printing speed at 10 mm/s. After choosing the pressure that led to the best resolution (2.8 bar), the printing speed was varied from 5 to 25 mm/s. The results obtained in these tests are presented in Figure 25.

Regarding the nozzle with a width of 0.20 mm, higher resolution filaments were obtained for an air pressure of 2.8 bar and printing speeds of 10 and 15 mm/s. However, its narrow width may endanger the viability of future loaded cells due to high pressure when extruded.[76,77] Along these lines, a final nozzle width of 0.25 mm was tested. For this nozzle's width, air pressure was again varied with a constant printing speed of 10 mm/s. The filament that presented the highest resolution was the one printed at a pressure of 2 bars. As follows, air pressure was maintained at 2 bar whilst the printing speed was varied from 5 to 25 mm/s. Figure 26 presents the results of the printing tests for this nozzle.

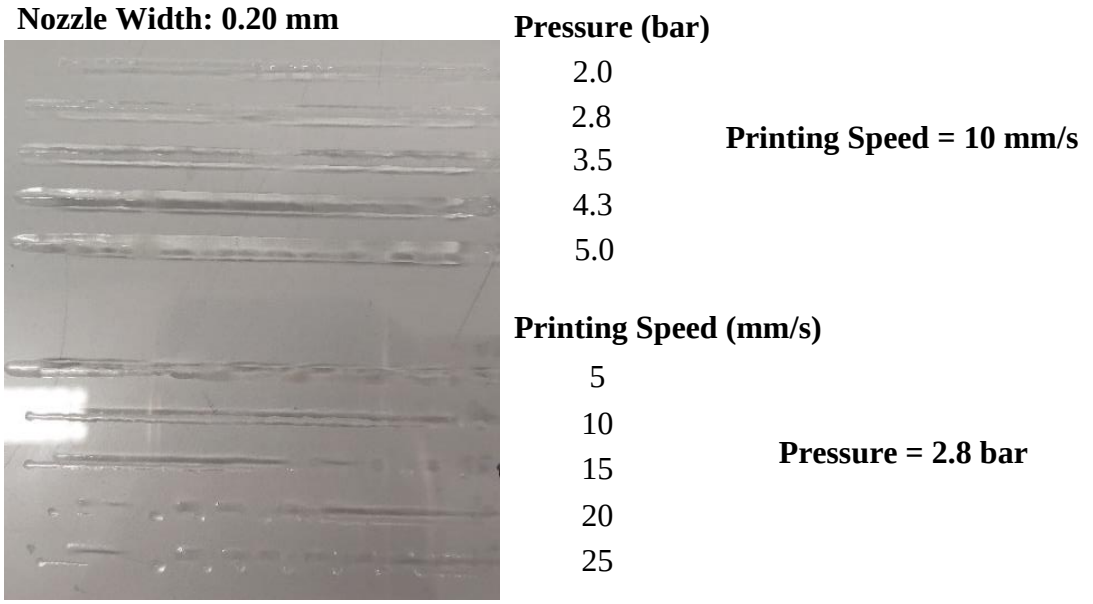

Figure 25 - Printing studies with the alginate 4% (w/v) ink using a nozzle with a width of 0.20 mm.

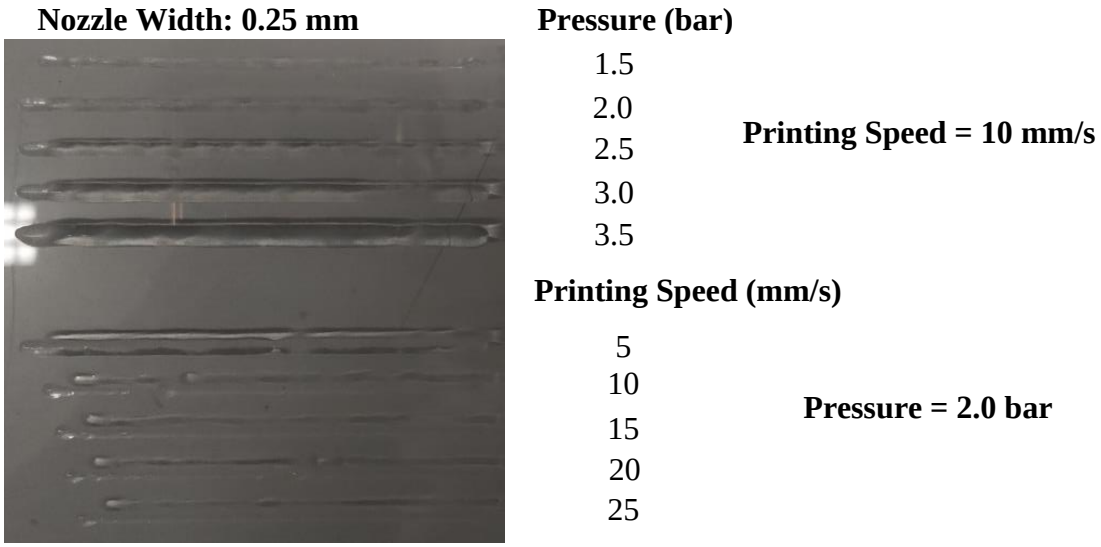

Figure 26 - Printing studies with the alginate 4% (w/v) ink using a nozzle with a width of 0.25 mm.

The best results were obtained for the nozzle with a width of 0.25 mm with a good balance between printing resolution, air pressure and printing speed, without extruding large quantities of ink, as the 0.41 mm nozzle width, neither applying high pressure as for the 0.20 mm nozzle width. An air pressure of 2 bar was chosen for this nozzle since it presented the highest resolution out of the variously air pressures tested. As for the printing speed, 10 mm/s

was chosen as the one leading to the best results since higher speeds led to filament break and lower speeds led to excessive quantities of extruded ink. An air pressure of 1.5 bar was also taken into account since even though it presented less resolution than the filament printed with a pressure of 2 bar, it was enough to print a well-defined filament.

Then, alginate and the alginate-microparticles inks were printed using the selected printing parameters (air pressure: 1.5 or 2 bar; printing speed:10 mm/s; nozzle width: 0.25 mm) and a more complex printed structure (1.5 mm between strands and 10 deposited layers) (Figure 15). The results for these printing assays are shown in Figure 27.

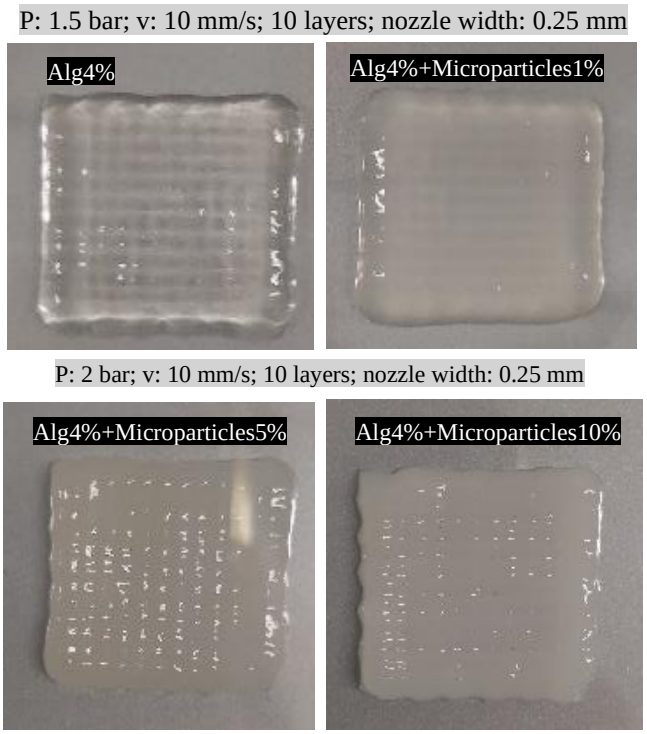

Figure 27 - Printed constructs of alginate and alginate-microparticles inks obtained using a 0.25 mm nozzle width and a space of 1.5 mm between ink strands.

The resulting structures presented low resolution since it was not possible to observe the space between strands, and therefore the gride structure. To achieve higher resolutions for the printed constructs, additional printing studies were carried out varying space between ink filaments. In these tests, the number of deposited layers was also varied.

5.2.3. Optimization of the printing parameters: 3D constructs

Expressly, the space between filaments was set at 1.5 mm, 2.25 mm and 3mm and the number of printed layers at 2, 4 or 6. The other printing parameters were an air pressure of 1.5 or 2 bar and a printing speed of 8.5 mm/s. For alginate and Alg4%+Microparticles1%, the construct with 6 layers was not fabricated since it was observed, when printing 2 or 4 layers, that the constructs have low resolution. In Figure 28 are presented the results of these tests for both alginate and alginate-microparticles inks.

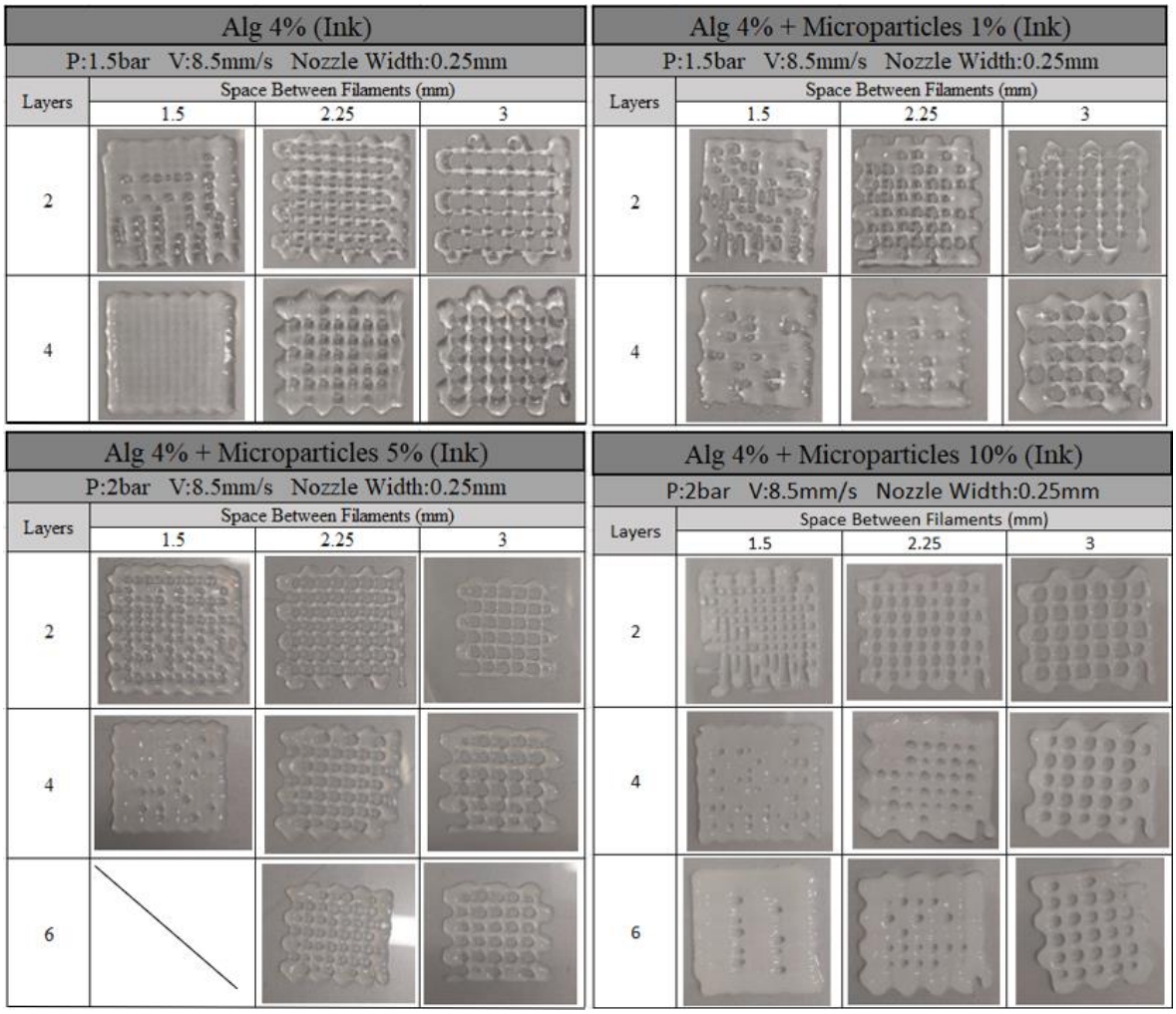

Figure 28 - Printing constructs of alginate and alginate-microparticles inks.

Regarding these results, Alg4% and Alg4%+Microparticles1% inks led to low resolution printed constructs since most do not maintain the pretended grid structure. On the contrary, Alg4%+Microparticles5% and Alg4%+Microparticles10% inks led to high resolution printed constructs with a space of 3 mm between construct filaments.

According to these results, a higher concentration of microparticles leads to better-printed constructs, indicating that the microparticles give firmness to the structure. Space between the construct filaments and the number of deposited layers are two critical factors to obtain high resolution. In this way, the structures which showed higher resolution (3mm space between filaments, with 4 and 6 layers of Alg4%+Microparticles5% and Alg4%+Microparticles10% inks) were cross-linked with a 0.5% (w/v) $CaCl_2$ solution. These fully cross-linked printed constructs are presented in Figure 29.

All the cross-linked constructs kept their structure upon being cross-linked. In this way, the optimal parameters to print higher resolution structures are air pressure: 2 bar; printing speed: 8.5 mm/s; nozzle width: 0.25 mm; space between strands: 3mm).

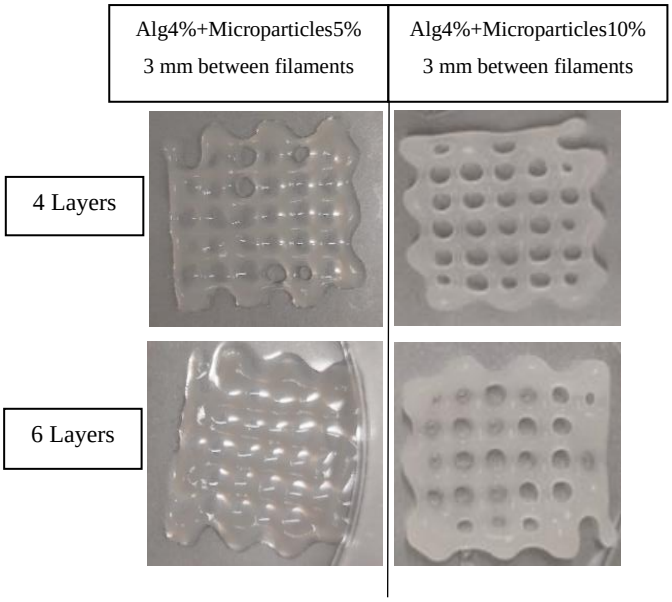

Figure 29 - Cross-linked structures obtained with Alg4%+Microparticles5% and Alg4%+Microparticles10% with four layers (top) and six layers (bottom) with 3mm space between filaments.

5.2.4. Scanning electron microscopy (SEM) of the printed constructs

In order to confirm the presence of microparticles in the printed constructs, SEM analysis of the constructs printed with the alginate inks containing 5% and 10% of microparticles was carried. Surface images of these constructs are presented in Figure 30.

The images show the presence of cellulose acetate microparticles in both samples. Moreover, it is also perceived that the microparticles were evenly distributed over the entire

surface of the construct and retained their original spherical form, not being damaged by the pressure applied during the extrusion printing.

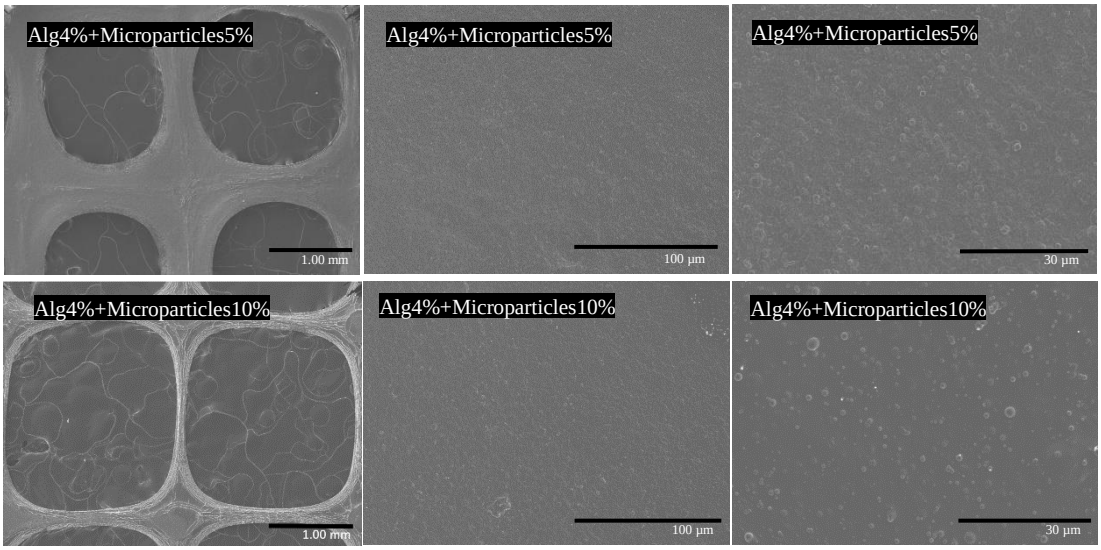

Figure 30 - Scanning electron microscopy (SEM) images of the surface of the 3D-printed constructs of alginate-microparticles hydrogels with 5% and 10% of CA microparticles.

The space between the printed constructs' filaments was determined using the ImageJ software, and the results are shown in Figure 31. Although the original constructs were printed with a space between filaments of 3 mm, this parameter is much smaller in the SEM micrographs. These differences are certainly associated with the spreading of the inks during printing and/or shrinkage of the constructs during drying.

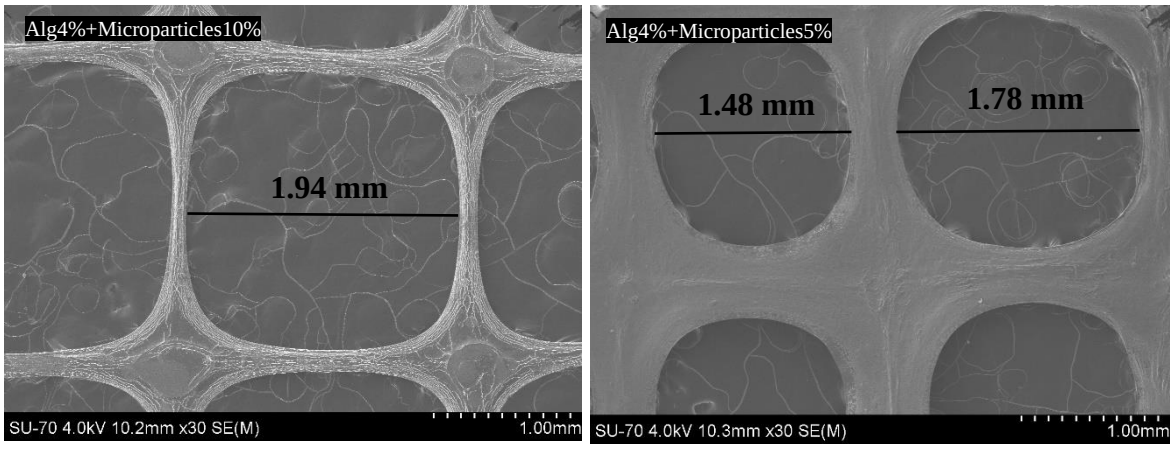

Figure 31 – SEM micrographs of the surface of the 3D-printed constructs of alginate-microparticles hydrogels with 5% and 10% of CA microparticles and respective measured space between filaments.

6. Conclusion and future perspectives

The objective of this work was the development of a novel biopolymeric microcarrier based bioink with improved mechanical properties and high cell viability for application in 3D-bioprinting. To achieve this goal, firstly, cellulose acetate microparticles were produced by dissolving cellulose acetate in acetone and regeneration following the water-on-polymer method. The obtained microparticles were characterized accordingly to their chemical structure and morphology, which proved to be spherical with an average size of 573.83±178.76 nm. The microparticles' suspension also revealed high cell viability towards HaCaT cells, with cell viability values over 75%. Then, various alginate-based inks were prepared by adding different amounts of cellulose acetate microparticles to the alginate solution to achieve concentrations of microparticles of 1%, 5% and 10% (m/m), followed by a pre-crosslinking step with a $CaCl_2$ solution. The viscosity and shear stress of the inks increased with the amount of microparticles, and all revealed a shear-thinning behaviour which is optimal for extrusion bioprinting. The G' and G" moduli of the fully cross-linked hydrogels (obtained after cross-link with a $CaCl_2$ solution) showed how the storage modulus was prevalent compared to the loss modulus revealing the consistency and solid-like behaviour of the printed structure, as well as confirming their complete reticulation. Then, the 3D printing process was optimized, and the best conditions were selected, namely a pressure of 2 bar, a printing speed of 8.5 or 10 mm/s, and a nozzle width of 0.25 mm. Upon carrying out printing tests to improve the resolution of the printed structures, the sample with the most promising result was the Alg4%+Microparticles10% ink, which allowed to print up to 6 layers with a space of 3 mm between strands of ink. The printed structures were fully cross-linked with a 0.5% (m/v) $CaCl_2$ solution, and the obtained constructs were analyzed by SEM, confirming the presence of the microparticles homogeneously distributed in the printed structures.

Even though the alginate-cellulose acetate inks revealed considerable potential for the 3D-bioprinting of living tissue, there are still important topics that require further studying, such as:

- Loading of the hydrogels with cells, and confirmation of their rheological properties and printability;
- Evaluation of the mechanical properties of the printed constructs by compression tests;

- Determination of the cell viability after the extrusion printing process;
- Investigation of the cell proliferation and tissue formation in 3D-bioprinted constructs;
- Investigation of the rate of degradation of the hydrogel compared to the formation of new tissue.

7. Bibliography

1. Jamee R, Araf Y, Naser I Bin, Promon SK. The promising rise of bioprinting in revolutionalizing medical science: Advances and possibilities. *Regen Ther*. 2021;18:133-145. doi:10.1016/j.reth.2021.05.006
2. Sánchez Rodríguez DA, Ramos-Murillo AI, Godoy-Silva RD. Tissue engineering, 3D-Bioprinting, morphogenesis modelling and simulation of biostructures: Relevance, underpinning biological principles and future trends. *Bioprinting*. 2021;24(August 2020):e00171. doi:10.1016/j.bprint.2021.e00171
3. Hospodiuk M, Dey M, Sosnoski D, Ozbolat IT. The bioink: A comprehensive review on bioprintable materials. *Biotechnol Adv*. 2017;35(2):217-239. doi:10.1016/j.biotechadv.2016.12.006
4. Lanza R, Langer R, Vacanti J. *Principles of Tissue Engineering*.; 2007. doi:10.1006/cryo.1999.2214
5. U.S. Department of Health & Human Services. Organ Procurement and Transplantation Network. https://optn.transplant.hrsa.gov/data/view-data-reports/national-data/#. Published 2020.
6. Wang P, Sun Y, Shi X, Shen H, Ning H, Liu H. Bioscaffolds embedded with regulatory modules for cell growth and tissue formation: A review. *Bioact Mater*. 2020;6(5):1283-1307. doi:10.1016/j.bioactmat.2020.10.014
7. Ma PX. Biomimetic materials for tissue engineering. *Adv Drug Deliv Rev*. 2008;60(2):184-198. doi:10.1016/j.addr.2007.08.041
8. Vacanti JP, Langer R. Tissue engineering: The design and fabrication of living replacement devices for surgical reconstruction and transplantation. *Lancet*. 1999;354(SUPPL.1):32-34. doi:10.1016/s0140-6736(99)90247-7
9. Burke JF, Yannas O V, Quinby WC, Bondoc CC, Jung WK. Successful use of a physiologically acceptable artificial skin in the treatment of extensive burn injury. *Ann Surg*. 1981;194(4):413-427. doi:10.1097/00000658-198110000-00005
10. Farhat W, Chatelain F, Marret A, Faivre L, Arakelian L, Cattan P, Fuchs A. Trends in 3D bioprinting for esophageal tissue repair and reconstruction. *Biomaterials*. 2020;267:120465. doi:10.1016/j.biomaterials.2020.120465
11. Zhou D, Chen J, Liu B, Zhang X, Li X, Xu T. Bioinks for jet-based bioprinting. *Bioprinting*. 2019;16(May):e00060. doi:10.1016/j.bprint.2019.e00060
12. Gu Z, Fu J, Lin H, He Y. Development of 3D bioprinting: From printing methods to biomedical applications. *Asian J Pharm Sci*. 2020;15(5):529-557. doi:10.1016/j.ajps.2019.11.003
13. Matai I, Kaur G, Seyedsalehi A, McClinton A, Laurencin CT. Progress in 3D bioprinting technology for tissue/organ regenerative engineering. *Biomaterials*. 2020;226(September 2019):119536. doi:10.1016/j.biomaterials.2019.119536
14. Bova L, Billi F, Cimetta E. Mini-review: advances in 3D bioprinting of vascularized constructs. *Biol Direct*. 2020;15(1):1-5. doi:10.1186/s13062-020-00273-4
15. Ozbolat IT, Hospodiuk M. Current advances and future perspectives in extrusion-based bioprinting. *Biomaterials*. 2016;76:321-343.

doi:10.1016/j.biomaterials.2015.10.076

16. Khalil S, Nam J, Sun W. Multi-nozzle deposition for construction of 3D biopolymer tissue scaffolds. *Rapid Prototyp J*. 2005;11(1):9-17. doi:10.1108/13552540510573347

17. Gary A. Fielding, Amit Bandyopadhyay SB. Effects of silica and zinc oxide doping on mechanical and biological properties of 3D printed tricalcium phosphate tissue engineering scaffolds. *Dent Mater*. 2012;28(2):113-122. https://doi.org/10.1016/j.dental.2011.09.010.

18. Visser J, Peters B, Burger TJ, Boomstra J, Dhert WJA, Melchels FPW, Malda J. Biofabrication of multi-material anatomically shaped tissue constructs. *Biofabrication*. 2013;5(3):035007. doi:10.1088/1758-5082/5/3/035007

19. Gudapati H, Dey M, Ozbolat I. A comprehensive review on droplet-based bioprinting: Past, present and future. *Biomaterials*. 2016;102:20-42. doi:10.1016/j.biomaterials.2016.06.012

20. Tan CT, Liang K, Ngo ZH, Dube CT, Lim CY. Application of 3d bioprinting technologies to the management and treatment of diabetic foot ulcers. *Biomedicines*. 2020;8(10):1-19. doi:10.3390/biomedicines8100441

21. Singh M, Haverinen HM, Dhagat P, Jabbour GE. Inkjet printing-process and its applications. *Adv Mater*. 2010;22(6):673-685. doi:10.1002/adma.200901141

22. Wijshoff H. The dynamics of the piezo inkjet printhead operation. *Phys Rep*. 2010;491(4-5):77-177. doi:10.1016/j.physrep.2010.03.003

23. Yu J, Park SA, Kim WD, Ha T, Xin YZ, Lee JH, Lee D. Current advances in 3D bioprinting technology and its applications for tissue engineering. *Polymers (Basel)*. 2020;12(12):1-30. doi:10.3390/polym12122958

24. Ozbolat IT, Yu Y. Bioprinting toward organ fabrication: Challenges and future trends. *IEEE Trans Biomed Eng*. 2013;60(3):691-699. doi:10.1109/TBME.2013.2243912

25. Donderwinkel I, Van Hest JCM, Cameron NR. Bio-inks for 3D bioprinting: Recent advances and future prospects. *Polym Chem*. 2017;8(31):4451-4471. doi:10.1039/c7py00826k

26. Murphy S V., Atala A. 3D bioprinting of tissues and organs. *Nat Biotechnol*. 2014;32(8):773-785. doi:10.1038/nbt.2958

27. Zhang P, Wang H, Wang P, Zheng Y, Liu L, Hu J, Liu Y, Gao Q, He Y. Lightweight 3D bioprinting with point by point photocuring. *Bioact Mater*. 2020;6(5):1402-1412. doi:10.1016/j.bioactmat.2020.10.023

28. Yang Y, Zhou Y, Lin X, Yang Q, Yang G. Printability of external and internal structures based on digital light processing 3D printing technique. *Pharmaceutics*. 2020;12(3). doi:10.3390/pharmaceutics12030207

29. Gopinathan J, Noh I. Recent trends in bioinks for 3D printing. *Biomater Res*. 2018;22(1):11. doi:10.1186/s40824-018-0122-1

30. Pahlevanzadeh F, Mokhtari H, Bakhsheshi-Rad HR, Emadi R, Kharaziha M, Valiani A, Poursamar SA, Ismail AF, RamaKrishna S, Berto F. *Recent Trends in Three-Dimensional Bioinks Based on Alginate for Biomedical Applications*. Vol 13.; 2020. doi:10.3390/ma13183980

31. Gungor-Ozkerim PS, Inci I, Zhang YS, Khademhosseini A, Dokmeci MR. Bioinks for 3D bioprinting: An overview. *Biomater Sci*. 2018;6(5):915-946. doi:10.1039/c7bm00765e

32. Khoshnood N, Zamanian A. A comprehensive review on scaffold-free bioinks for bioprinting. *Bioprinting*. 2020;19(February):e00088. doi:10.1016/j.bprint.2020.e00088

33. Schrobback K, Klein TJ, Crawford R, Upton Z, Malda J, Leavesley DI. Effects of oxygen and culture system on in vitro propagation and redifferentiation of osteoarthritic human articular chondrocytes. *Cell Tissue Res*. 2012;347(3):649-663. doi:10.1007/s00441-011-1193-7

34. Yu Y, Moncal KK, Li J, Peng W, Rivero I, Martin JA, Ozbolat IT. Three-dimensional bioprinting using self-Assembling scalable scaffold-free "tissue strands" as a new bioink. *Sci Rep*. 2016;6(June):1-11. doi:10.1038/srep28714

35. Nuttelman CR, Rice MA, Rydholm AE, Salinas CN, Shah DN, Anseth KS. Macromolecular monomers for the synthesis of hydrogel niches and their application in cell encapsulation and tissue engineering. *Prog Polym Sci*. 2008;33(2):167-179. doi:10.1016/j.progpolymsci.2007.09.006

36. Catoira MC, Fusaro L, Di Francesco D, Ramella M, Boccafoschi F. Overview of natural hydrogels for regenerative medicine applications. *J Mater Sci Mater Med*. 2019;30(10). doi:10.1007/s10856-019-6318-7

37. Ramiah P, du Toit LC, Choonara YE, Kondiah PPD, Pillay V. Hydrogel-Based Bioinks for 3D Bioprinting in Tissue Regeneration. *Front Mater*. 2020;7(April):1-13. doi:10.3389/fmats.2020.00076

38. Li J, Wu C, Chu PK, Gelinsky M. 3D printing of hydrogels: Rational design strategies and emerging biomedical applications. *Mater Sci Eng R Reports*. 2020;140(January):100543. doi:10.1016/j.mser.2020.100543

39. Hu W, Wang Z, Xiao Y, Zhang S, Wang J. Advances in cross-linking strategies of biomedical hydrogels. *Biomater Sci*. 2019;7(3):843-855. doi:10.1039/c8bm01246f

40. O'Sullivan A, Howard K, Sueoka N. Location of a unique replication terminus and genetic evidence for partial bidirectional replication in the Bacillus subtilis chromosome. *J Mol Biol*. 1975;91(1):15-38. doi:10.1016/0022-2836(75)90369-1

41. Gasperini L, Mano JF, Reis RL. Natural polymers for the microencapsulation of cells. *J R Soc Interface*. 2014;11(100). doi:10.1098/rsif.2014.0817

42. Maranchi JP, Trexler MM, Guo Q, Elisseeff JH. Fibre-reinforced hydrogels with high optical transparency. *Int Mater Rev*. 2014;59(5):264-296. doi:10.1179/1743280414Y.0000000032

43. Klemm D, Heublein B, Fink HP, Bohn A. Cellulose: Fascinating biopolymer and sustainable raw material. *Angew Chemie - Int Ed*. 2005;44(22):3358-3393. doi:10.1002/anie.200460587

44. Wei W, Ma Y, Yao X, Zhou W, Wang X, Li C, Lin J, He Q, Leptihn S, Ouyang H. Advanced hydrogels for the repair of cartilage defects and regeneration. *Bioact Mater*. 2021;6(4):998-1011. doi:10.1016/j.bioactmat.2020.09.030

45. Hickey RJ, Pelling AE. Cellulose biomaterials for tissue engineering. *Front Bioeng*

Biotechnol. 2019;7(MAR):1-15. doi:10.3389/fbioe.2019.00045

46. Rees A, Powell LC, Chinga-Carrasco G, Gethin DT, Syverud K, Hill KE, Thomas DW. 3D bioprinting of carboxymethylated-periodate oxidized nanocellulose constructs for wound dressing applications. *Biomed Res Int*. 2015;2015. doi:10.1155/2015/925757

47. Portela R, Leal CR, Almeida PL, Sobral RG. Bacterial cellulose: a versatile biopolymer for wound dressing applications. *Microb Biotechnol*. 2019;12(4):586-610. doi:10.1111/1751-7915.13392

48. Markstedt K, Mantas A, Tournier I, Martínez Ávila H, Hägg D, Gatenholm P. 3D bioprinting human chondrocytes with nanocellulose-alginate bioink for cartilage tissue engineering applications. *Biomacromolecules*. 2015;16(5):1489-1496. doi:10.1021/acs.biomac.5b00188

49. Mendibil U, Ruiz-Hernandez R, Retegi-Carrion S, Garcia-Urquia N, Olalde-Graells B, Abarrategi A. Tissue-specific decellularization methods: Rationale and strategies to achieve regenerative compounds. *Int J Mol Sci*. 2020;21(15):1-29. doi:10.3390/ijms21155447

50. Gilpin A, Yang Y. Decellularization Strategies for Regenerative Medicine: From Processing Techniques to Applications. *Biomed Res Int*. 2017;2017. doi:10.1155/2017/9831534

51. Pati F, Jang J, Ha DH, Kim SW, Rhie JW, Shim JH, Kim DK, Cho DW. Printing three-dimensional tissue analogues with decellularized extracellular matrix bioink. *Nat Commun*. 2014;5. doi:10.1038/ncomms4935

52. Pati F, Ha DH, Jang J, Han HH, Rhie JW, Cho DW. Biomimetic 3D tissue printing for soft tissue regeneration. *Biomaterials*. 2015;62:164-175. doi:10.1016/j.biomaterials.2015.05.043

53. Malda J, Frondoza CG. Microcarriers in the engineering of cartilage and bone. *Trends Biotechnol*. 2006;24(7):299-304. doi:10.1016/j.tibtech.2006.04.009

54. Tavassoli H, Alhosseini SN, Tay A, Chan PPY, Weng Oh SK, Warkiani ME. Large-scale production of stem cells utilizing microcarriers: A biomaterials engineering perspective from academic research to commercialized products. *Biomaterials*. 2018;181:333-346. doi:10.1016/j.biomaterials.2018.07.016

55. Levato R, Visser J, Planell JA, Engel E, Malda J, Mateos-Timoneda MA. Biofabrication of tissue constructs by 3D bioprinting of cell-laden microcarriers. *Biofabrication*. 2014;6(3). doi:10.1088/1758-5082/6/3/035020

56. Kulchar RJ, Denzer BR, Chavre BM, Takegami M, Patterson J. A review of the use of microparticles for cartilage tissue engineering. *Int J Mol Sci*. 2021;22(19). doi:10.3390/ijms221910292

57. Neto MD, Oliveira MB, Mano JF. Microparticles in Contact with Cells: From Carriers to Multifunctional Tissue Modulators. *Trends Biotechnol*. 2019;37(9):1011-1028. doi:10.1016/j.tibtech.2019.02.008

58. Petzold-welcke HWK, Fardim P, Heinze T. Nanoparticles from conventional cellulose esters : evaluation of preparation methods. 2013:751-760. doi:10.1007/s10570-013-9874-x

59. Yeo MG, Ha JH, Lee HJ, Kim GH. Fabrication of hASCs-laden structures using extrusion-based cell printing supplemented with an electric field. *Acta Biomater*. 2016;38:33-43. doi:10.1016/j.actbio.2016.04.017

60. Horn D, Rieger J. Organic nanoparticles in the aqueous phase - Theory, experiment, and use. *Angew Chemie - Int Ed*. 2001;40(23):4330-4361. doi:10.1002/1521-3773(20011203)40:23<4330::AID-ANIE4330>3.0.CO;2-W

61. Stevulova N, Hospodarova V, Estokova A, Singovska E. Characterization of manmade and recycled cellulosic fibers for their application in building materials. *J Renew Mater*. 2019;7(11):1121-1145. doi:10.32604/jrm.2019.07556

62. Jahedi E, Panahi R. Conversion of lignocellulosic waste into effective flocculants: synthesis, characterization, and performance. *Bioresour Bioprocess*. 2021;8(1):1-12. doi:10.1186/s40643-021-00422-1

63. Zhuang J, Li M, Pu Y, Ragauskas AJ, Yoo CG. Observation of potential contaminants in processed biomass using fourier transform infrared spectroscopy. *Appl Sci*. 2020;10(12):1-13. doi:10.3390/app10124345

64. Nandiyanto ABD, Oktiani R, Ragadhita R. How to read and interpret ftir spectroscope of organic material. *Indones J Sci Technol*. 2019;4(1):97-118. doi:10.17509/ijost.v4i1.15806

65. Shao MH, Cui B, Zheng TF, Wang CH. Ultrasonic manipulation of cells for alleviating the clogging of extrusion-based bioprinting nozzles. *J Phys Conf Ser*. 2021;1798(1). doi:10.1088/1742-6596/1798/1/012009

66. Carvalho JPF, Silva ACQ, Silvestre AJD, Freire CSR, Vilela C. Spherical Cellulose Micro and Nanoparticles: A Review of Recent Developments and Applications. *Nanomaterials*. 2021;11(10):2744. doi:10.3390/nano11102744

67. Nunes MO, Fátima Goebel de Souza T de, Pierdoná TM, Ramos MV, Ferreira KQ, Duarte RS, Shahwar DE, Wilke DV, Wong DVT, Alencar NMN. In vitro biocompatibility and wound healing properties of latex proteins dressing. *Toxicol Vitr*. 2021;76(May). doi:10.1016/j.tiv.2021.105230

68. Ajdary R, Huan S, Zanjanizadeh Ezazi N, Xiang W, Grande R, Santos HA, Rojas OJ. Acetylated Nanocellulose for Single-Component Bioinks and Cell Proliferation on 3D-Printed Scaffolds. *Biomacromolecules*. 2019;20(7):2770-2778. doi:10.1021/acs.biomac.9b00527

69. Schwab A, Levato R, D'Este M, Piluso S, Eglin D, Malda J. Printability and Shape Fidelity of Bioinks in 3D Bioprinting. *Chem Rev*. 2020;120(19):11028-11055. doi:10.1021/acs.chemrev.0c00084

70. Kuipers B, van den Dobbelsteen G, Wedege E, van Alphen L. Serological Characterization. *Meningococcal Dis*. 2003:131-145. doi:10.1385/1-59259-149-3:131

71. Heggset EB, Strand BL, Sundby KW, Simon S, Chinga-Carrasco G, Syverud K. Viscoelastic properties of nanocellulose based inks for 3D printing and mechanical properties of CNF/alginate biocomposite gels. *Cellulose*. 2019;26(1):581-595. doi:10.1007/s10570-018-2142-3

72. Paxton N, Smolan W, Böck T, Melchels F, Groll J, Jungst T. Proposal to assess

printability of bioinks for extrusion-based bioprinting and evaluation of rheological properties governing bioprintability. *Biofabrication*. 2017;9(4):044107. doi:10.1088/1758-5090/aa8dd8

73. Hazur J, Detsch R, Karakaya E, Kaschta J, Teßmar J, Schneidereit D, Friedrich O, Schubert DK, Boccaccini AR. Improving alginate printability for biofabrication: establishment of a universal and homogeneous pre-crosslinking technique. *Biofabrication*. 2020;12(4). doi:10.1088/1758-5090/ab98e5

74. Kiyotake EA, Douglas AW, Thomas EE, Nimmo SL, Detamore MS. Development and quantitative characterization of the precursor rheology of hyaluronic acid hydrogels for bioprinting. *Acta Biomater*. 2019;95:176-187. doi:10.1016/j.actbio.2019.01.041

75. Hossain L, Raghuwanshi VS, Tanner J, Garnier G. Modulating nanocellulose hydrogels and cryogels strength by cross-linking and blending. *Colloids Surfaces A Physicochem Eng Asp*. 2021;630(September):127608. doi:10.1016/j.colsurfa.2021.127608

76. Chang R, Nam J, Sun W. Effects of dispensing pressure and nozzle diameter on cell survival from solid freeform fabrication-based direct cell writing. *Tissue Eng - Part A*. 2008;14(1):41-48. doi:10.1089/ten.a.2007.0004

77. Nair K, Gandhi M, Khalil S, Yan KC, Marcolongo M, Barbee K, Sun W. Characterization of cell viability during bioprinting processes. *Biotechnol J*. 2009;4(8):1168-1177. doi:10.1002/biot.200900004